DIELECTRIC BEHAVIOUR OF SOLID HYDROGEN IODIDE AND HYDROGEN BROMIDE AT FREQUENCIES BETWEEN 5 MHz AND 225 MHz

P. P. M. GROENEWEGEN

DIELECTRIC BEHAVIOUR OF SOLID HYDROGEN IODIDE AND HYDROGEN BROMIDE AT FREQUENCIES BETWEEN 5 MHz AND 225 MHz

PROEFSCHRIFT

TER VERKRIJGING VAN DE GRAAD VAN DOCTOR IN DE WISKUNDE EN NATUURWETENSCHAPPEN AAN DE RIJKSUNIVERSITEIT TE LEIDEN OP GEZAG VAN DE RECTOR MAGNIFICUS DR K. A. H. HIDDING, HOOGLERAAR IN DE FACULTEIT DER GODGELEERDHEID, TEN OVERSTAAN VAN EEN COMMISSIE UIT DE SENAAT TE VERDEDIGEN OP WOENSDAG 26 OKTOBER 1966 TE 15 UUR

DOOR

PAULUS PETRUS MARIA GROENEWEGEN
GEBOREN TE HEERLEN IN 1939

DRUCO DRUKKERIJBEDRIJVEN N.V. — LEIDEN

Promotor: Prof. Dr. C.J.F. Böttcher

Aan mijn ouders

Aan Henny

CONTENTS

CONTENTS

INTRODUCTION

Investigation of polar matter under application of a time dependent electromagnetic field of relatively large wavelength may provide information about the dynamical behaviour of electrostatically interacting molecules. In the usual case of sinusoidal time dependence of the applied field this information can conveniently be expressed by introducing the complex dielectric constant. Although experimentally numerous compounds have been investigated, most of the information obtained has so far resisted satisfactory interpretation as the necessary theoretical understanding of the underlying molecular processes is obstructed by incomplete knowledge of intra- and intermolecular structures.

In view of this state of affairs the investigation of solid hydrogen halides is of considerable interest. Diatomic molecules are comparatively simple and the symmetry properties of crystal lattices are attractive for intermolecular structure considerations. Nevertheless even these seemingly simple systems show a complicated dielectric behaviour with features often encountered in other cases which have so far resisted molecular explanation.

The present work contributes information about the dielectric behaviour of solid hydrogen iodide and hydrogen bromide at higher frequencies and higher temperatures than have been investigated before.

In the first chapter the theoretical background of the concepts and quantities commonly used for description of dielectric relaxation phenomena is discussed in an introductory manner. For application in subsequent chapters a review of experimental information on solid hydrogen iodide and hydrogen bromide is given. A simple model for an antiferroelectric solid phase transition due to dipole interaction is treated on basis of classical equilibrium statistical mechanics. The static dielectric properties of the model, as applied to hydrogen bromide, are derived.

In the second chapter the various parts of the measuring apparatus used for the determination of the presented dielectric data are discussed. Problems associated with the use of coupling leads between the measuring instrument and the unknown component are considered in some detail. Sample contraction effects affecting the quantitative significance of the experimental results are examined.

Results of admittance measurements on solid samples of hydrogen iodide and hydrogen bromide are given in the first two sections of the third chapter. At the available frequencies of investigation, relaxation behaviour could be measured in the temperature range of 80°K to 100°K. The major effort has been directed towards graphical representation of the results, as the well-established qualitative evidence is shown most clearly in this way. The observed frequency dependence of the dielectric constant of both compounds investigated can be represented within experimental error by the empirical skewed arc function, and best fit parameters are listed. In section 3-3 the accuracy of the results is discussed. The principal features of dielectric relaxation behaviour as shown by the data are summarized and possibilities of interpretation considered. From the results it appears that the dynamical behaviour in the higher temperature phases shows some resemblance to that observed for a variety of polar liquids. The evidence obtained further indicates that the change in cooperative molecular dynamics associated with the lowest, λ-type, phase transition is a long range order effect. The experimental information obtained is compared with some theories advanced for explanation of the dielectric behaviour of hydrogen halides or solids in general.

CHAPTER 1

THEORETICAL CONSIDERATIONS

1-1. ON THE THEORY OF DIELECTRIC RELAXATION

The following outline of the phenomenological and the statistical mechanical theory of dielectric relaxation aims at the systematic introduction of the various concepts that bear relevance to the subject of the present investigation, the dielectric behaviour of solid hydrogen halides.

PHENOMENOLOGICAL

Basis for the phenomenological description of the behaviour of ponderable matter in an electromagnetic field are Maxwell's equations. These partial differential equations relate the macroscopic field vectors $\mathbf{E}(\mathbf{R},t)$, $\mathbf{B}(\mathbf{R},t)$, $\mathbf{D}(\mathbf{R},t)$, $\mathbf{H}(\mathbf{R},t)$, called the electric and magnetic field intensity and the electric and magnetic displacement respectively, to the macroscopic charge and current densities $\rho(\mathbf{R},t)$ and $\mathbf{i}(\mathbf{R},t)$. Additional so-called constitutive relations for the quantities introduced may hold depending on the properties of the material under consideration, and serve to classify materials. So a homogeneous material is called a lineair dielectric if the relations

$$\rho(\mathbf{R},t) = 0, \quad \mathbf{i}(\mathbf{R},t) = 0, \quad \mathbf{B}(\mathbf{R},t) - \mathbf{H}(\mathbf{R},t) = 0 \qquad (1\text{-}1abc)$$

$$\mathbf{D}(\mathbf{R},t) - \mathbf{E}(\mathbf{R},t) = \int_{-\infty}^{t} f(t-\tau)\mathbf{E}(\mathbf{R},\tau)d\tau \qquad (1\text{-}1d)$$

hold at uniform temperature and pressure. The fourth relation expresses the linearity of the dielectric and implies the applicability of the principles of causality and linear superposition of after-effects for stimulus-response phenomena. The function f, which we call after-effect function, depends on time

but does not depend on E in the presupposed linear approximation, implying that the field strenghts considered are sufficiently small. The dependence of f on molecular parameters falls outside the scope of the phenomenological theory. For uniform temperature and density , $f(\rho,T,t)$ is independent of the position vector **R**. For anisotropic media the function f is a second rank tensor, reducing to a scalar for isotropic media.

Because of the causality condition, the integration in eq. (1-1d) extends only over values of $f(t)$ for $t > 0$, leaving us free to define

$$f(t) = 0 \quad \text{for } t < 0 \tag{1-2}$$

We next assume, that $f(t)$, as defined by eqs. (1-1d) and (1-2), has a Fourier transform $\hat{f}(\omega)$

$$\hat{f}(\omega) = \int_{-\infty}^{+\infty} f(t) e^{i\omega t} dt \tag{1-3a}$$

$$f(t) = \frac{1}{2\pi} \int_{-\infty}^{+\infty} \hat{f}(\omega) e^{-i\omega t} d\omega \tag{1-3b}$$

and take the transform of eq. (1-1d)

$$\hat{\mathbf{P}}(\mathbf{R},\omega) = \hat{f}(\omega)\hat{\mathbf{E}}(\mathbf{R},\omega) \tag{1-4}$$

where $\mathbf{P}(\mathbf{R},t) = \mathbf{D}(\mathbf{R},t) - \mathbf{E}(\mathbf{R},t)$ is called the electric polarization. The lower limit of integration in eq. (1-3a) may be replaced by 0 because of (1-2). This allows for derivation of symmetry relations and Kramers-Kronig relations[1] for $\hat{f}(\omega)$, which are consequences of the causality condition.

With the aid of eq. (1-4) we calculate the response $\mathbf{P}(\mathbf{R},t)$ to a sinusoidal field

$$\mathbf{E}(\mathbf{R},t) = \mathbf{E}_0(\mathbf{R}) e^{i\omega_0 t} \tag{1-5}$$

as

$$\mathbf{P}(\mathbf{R},t) = f(-\omega_0)\mathbf{E}(\mathbf{R},t) \tag{1-6}$$

Eqs. (1-5) and (1-6) are usually taken to define $\chi(\omega) = \hat{f}(-\omega)$, the dielectric susceptibility, and $\epsilon(\omega) = 1 + \chi(\omega)$, the dielectric permeability or complex dielectric constant. Adopting the customary convention, to write $\epsilon(\omega) = \epsilon'(\omega) - i\epsilon''(\omega)$ we obtain

$$\epsilon'(\omega) = 1 + \hat{f}'(\omega) \text{ and } \epsilon''(\omega) = \hat{f}''(\omega) \qquad (1\text{-}7)$$

The quantity $\epsilon_o = \epsilon(0)$ is called the static dielectric constant, being the constant of proportionality between **D** and **E** for static fields.

This concludes the formal treatment based on the superposition integral (1-1d). The dielectric permeability will, like $f(t)$, be a scalar function of density and temperature for isotropic media.

Before proceeding to discuss the representation of experimental $\epsilon(\omega)$ data, we introduce a few more concepts. From physical considerations, we deduce that the after-effect function $f(t)$ is related to various kinds of microscopic processes which may be divided in fast and slow ones with respect to the time scale of dielectric measurements, i.e. $t > 10^{-12}$ sec. Assuming their effect to be additive, we write $f(t) = f_1(t) + f_2(t)$, where $f_1(t)$ is different from zero only for $t < t_1 < 10^{-12}$ and $f_2(t)$, extending over much longer times, refers to dielectric relaxation proper. Consequently, the treatment given above, may be repeated for both f_1 and f_2 individually, leading to separate dispersion relations for $\hat{f}_1(\omega)$ and $\hat{f}_2(\omega)$. This enables us to introduce for dielectric phenomena ($\omega < 10^{12}$) the quantity

$$\hat{f}_1(\omega) \approx \int_o^{t_1} f_1(t) e^{i\omega t} dt \approx \int_o^{t_1} f_1(t) dt \approx \int_o^{\sim} f_1(t) dt = \epsilon_{\sim} - 1 \qquad (1\text{-}8)$$

where $\epsilon_{\sim}$ is called the high frequency dielectric constant.

Experimentally, a variety of functional dependences of $\epsilon(\rho, T, \omega)$ have been observed for different kinds of materials. Empirical formulae, describing explicitly the frequency dependence of ϵ, have been found to represent, in appreciable temperature ranges, experimental data of particular substances within experimental error. Of these we mention

$$\epsilon(\omega) = \epsilon_\infty + \frac{\epsilon_o - \epsilon_\infty}{1 + i\omega\tau_d} \qquad (1\text{-}9a)$$

$$\epsilon(\omega) = \epsilon_\infty + \frac{\epsilon_o - \epsilon_\infty}{1 + (i\omega\tau_{ca})^{1-\alpha}} \quad , \; 0 \leqq \alpha < 1 \qquad (1\text{-}9b)$$

$$\epsilon(\omega) = \epsilon_\infty + \frac{\epsilon_o - \epsilon_\infty}{(1 + i\omega\tau_{sa})^{\beta}} \quad , \; 0 < \beta \leqq 1 \qquad (1\text{-}9c)$$

The Cole-Cole plots, i.e. the graphical representation of $\epsilon''(\omega)$ vs. $\epsilon'(\omega)$ at constant density and temperature, corresponding to the formulae (1-9) have been named after their shapes, resp. semicircle, circular arc[2] and skewed arc[3].

Dielectrics, of which the dispersion may be described with formula (1-9a), are said to display Debije behaviour[4]. The after effect function $f_2(t)$ corresponding to (1-9a) is found to be proportional to $\exp(-t/\tau_d)$ so that τ_d is a measure for the time necessary for appreciable decay. A parameter τ occurring in a product $i\omega\tau$ in a dispersion formula (cf. (1-9)) is called a characteristic or relaxation time.

The simple expression for $f_2(t)$ in the case of Debije behaviour has led to the introduction of continuous or discrete distribution functions $F(k)$ of relaxation rates $k = \tau^{-1}$

$$f_2(t) = \int_0^{\sim} F(k) e^{-kt}\, dk \qquad (1\text{-}10)$$

in order to describe more complicated behaviour. Because of the assumption on $f_2(t)$ mentioned earlier, the description (1-10) is always possible. When an empirical formula is found to represent certain $\epsilon(\omega)$ data, the associated functions $f_2(t)$ and $F(k)$ may be calculated, as has been done for eqs. (1-9b) and (1-9c)[2,3].

Finally the following may be said about the presentation of dielectric data, confining ourselves to condensed phases at normal pressure, in which case the ρ-dependence of ϵ may be included in the T-dependence. Pairs of numbers $\epsilon'(\omega, T)$ and $\epsilon''(\omega, T)$ are

obtained from measurements over certain frequency and temperature ranges. Graphical representation of constant temperature measurements in a Cole-Cole plot will be helpful in deciding whether some empirical formula might describe the frequency dependence. By comparison of all observed data with ones, calculated by means of a suitable empirical formula with optimal parameters, it is decided whether this formula is representative. The merit of empirical formulae like (1-9b) and (1-9c) is mainly to be found in their ability to represent experimental data with the aid of only a few (temperature dependent) parameters.

STATISTICAL MECHANICAL

An explanation of the macroscopic dielectric behaviour of matter will require knowledge of the relevant molecular processes. Statistical mechanics provides the formal framework for obtaining macroscopic quantities by proper averaging of the microscopic phenomena represented by some profitable model.

In order to introduce the concept of electric moments, a molecule is considered to be a collection of point particles with electric charges $e_i (i=1,\ldots,n)$. The coordinates $\mathbf{r}_i$ denote the positions of the particles with respect to a reference point within the molecule. Then the electric multipole moments of the molecule with respect to the chosen reference point are defined

$$\sum_i e_i = e \quad , \text{ unipole moment (charge)} \qquad (1\text{-}11a)$$

$$\sum_i e_i \mathbf{r}_i = \mathbf{m} \quad , \text{ dipole moment} \qquad (1\text{-}11b)$$

with expressions for tensors of increasing rank defining higher order multipole moments.

Now we consider a system of volume V consisting of N neutral molecules ($e=0$ and $\mathbf{m}$ is independent of the choice of the reference point) labeled with index k. We let the reference point of the k^{th} molecule be its center of gravity with position coordinate $\mathbf{R}_k$. Thus we have for the set of canonically conjugated position and momentum coordinates: $(\mathbf{R}_k, \mathbf{r}_{ki})$ and $(\mathbf{p}_k, \mathbf{p}_{ki})$. Then, considering

a molecule to contribute to the macroscopic electric multipole density at position $\mathbf{R}$ at time t, when its centre of gravity $\mathbf{R}_k$ is located at $\mathbf{R}$, we obtain for the dipole moment density[5]

$$\mathbf{P}(\mathbf{R},t) = \langle \sum_k \mathbf{m}_k \, \delta(\mathbf{R}_k - \mathbf{R}) f \rangle \qquad (1\text{-}12)$$

where f is the normalized probability distribution function and $\langle\ \rangle$ indicates integration over phase space.

A straightforward derivation of Maxwell's macroscopic equations from Lorentz's microscopic ones on the basis of ensemble averaging[5] shows that the dipole moment density $\mathbf{P}(\mathbf{R},t)$ may be identified with the electric polarization $\mathbf{D}(\mathbf{R},t)-\mathbf{E}(\mathbf{R},t)$ introduced in the phenomenological treatment, if terms involving higher moment densities may be neglected. This we will assume to be justified.

The statistical mechanical derivation of the superposition integral (1-1d) in its general form is still lacking, i.e. the justification that ϵ is independent of the position vector $\mathbf{R}$ for uniform density and temperature. Kubo's formalism[6], a perturbation treatment for the linear response of a system to a weak external force, the effect of which may be represented by an additional term in the Hamiltonian of the system, has been applied to dielectric relaxation[7,8]. In this case, the perturbation term in the Hamiltonian is

$$H' = -\mathbf{M}.\mathbf{E}_0(t) \quad , \quad \mathbf{M} = \sum_k \mathbf{m}_k \qquad (1\text{-}13)$$

where the applied electric field $\mathbf{E}_0(t)$ is uniform throughout the system (thus requiring that the wavelength associated with the time dependence of $\mathbf{E}_0(t)$ is large compared with the diameter of the system). At present we introduce the assumption that the system has translational symmetry irrespective of the presence of $\mathbf{E}_0(t)$; hence we impose restrictions on the shape of the system. Then the dipole moment density $\mathbf{P}(t)$ is independent of the position vector $\mathbf{R}$. In the case of a crystal this implies that $\mathbf{P}(\mathbf{R},t)$ as defined by eq. (1-12) is replaced by its volume average over at least one unit cell. Further in the case of an anisotropic crystal

we somehow fix its macroscopic orientation to avoid complications due to rotation of the system under influence of the applied field. The treatment then proceeds to determine the perturbation term for the time dependent distribution function $f(t)$ linear in $\mathbf{E}_0(t)$, and the average total moment of the system, which we assume to vanish for $\mathbf{E}_0 = 0$, becomes

$$\bar{\mathbf{M}}(t) = \mathbf{P}(t)V = < \mathbf{M}f > = \int_0^{\infty} d\tau \; (-\dot{\bar{\Phi}}(\tau))\mathbf{E}_0(t-\tau) \tag{1-14}$$

with the following expression for the tensor elements of the correlation function $\bar{\Phi}(t)$ (moment in μ-direction when the applied field is in the ν-direction)

$$\bar{\Phi}_{\mu\nu}(t) = \beta < M_\mu(0)M_\nu(t)f^o > \quad , \; \beta = 1/kT \tag{1-15}$$

In the expression (1-15) the zero superscript in f^o indicates that the average is taken over the unperturbed system and $\mathbf{M}(t)$ denotes the implicit time dependence of $\mathbf{M}$ through the natural motion of the system. Taking the Fourier transform of eq. (1-14) we obtain the admittance of the system.

In order to arrive at an expression for the dielectric susceptibility as defined by eqs. (1-5) and (1-6) we approximate the macroscopic field intensity $\mathbf{E}$ that enters into Maxwell's equations with the ensemble average[9]

$$\begin{aligned} \mathbf{E}(t) &= \mathbf{E}_0(t) + < \sum_k T(\mathbf{R}, \mathbf{R}_k)\, \mathbf{m}_k f > \\ &= \mathbf{E}_0(t) + \int_V d\mathbf{R}' \; T(\mathbf{R}, \mathbf{R}')\, \mathbf{P}(t) \\ &= \mathbf{E}_0(t) - A\, \mathbf{P}(t) \end{aligned} \tag{1-16}$$

where $T(\mathbf{R}, \mathbf{R}_k)\, \mathbf{m}_k(\mathbf{R}_k)$ is the negative gradient at $\mathbf{R}$ of the scalar potential at $\mathbf{R}$ due to the point dipole $\mathbf{m}_k$ at $\mathbf{R}_k$. The field $\mathbf{E}(t)$ as well as is the depolarization tensor A again are independent of $\mathbf{R}$ because of translational symmetry. Combining eqs. (1-14) and

(1-16) and taking Fourier transforms we obtain for the dielectric susceptibility tensor

$$\chi(\omega) = \frac{\kappa(\omega)}{I - A\kappa(\omega)} \tag{1-17}$$

$$\kappa(\omega) = \frac{1}{V}\int_0^{\sim} dt\ e^{i\omega t}\ \{-\dot{\Phi}(t)\} \tag{1-18}$$

where I is the unit tensor. For $\det(I - A\kappa(0)) > 0$ the susceptibility $\chi(\omega)$ will, like $\kappa(\omega)$[6,9], obey symmetry relations and Kramers-Kronig relations. When the difference between the adiabatic and isothermal susceptibility may be neglected, $\chi(\omega)$ may be identified with the phenomenological measurable susceptibility introduced before. The main unsatisfactory feature of the result obtained is that it does not show how the two shape dependent quantities A and κ combine to give a shape independent material constant χ.

As in the phenomenological treatment a high frequency dielectric constant $\epsilon_\sim = \chi_\sim + 1$ may be generated by separating from $\dot{\Phi}(t)$ a rapidly decaying term. This permits us to write eq. (1-17) in an alternative form

$$\frac{\epsilon(\omega) - \epsilon_\sim}{\epsilon_0 - \epsilon_\sim} = \left\{1 + \frac{I - A\kappa_\sim}{I - A\kappa_0}\left[\left(\frac{\kappa(\omega) - \kappa_\sim}{\kappa_0 - \kappa_\sim}\right) - 1\right]\right\}^{-1} \tag{1-17a}$$

which in the case of an isotropic sample of spherical shape ($A = 1/3$[10]) coincides with formulae given by Glarum[7] and Cole[8], who also consider the consequences of theories reducing $\dot{\Phi}$ to restricted correlation functions referring to localized moments.

1-2. AVAILABLE EXPERIMENTAL INFORMATION ON HYDROGEN IODIDE AND HYDROGEN BROMIDE

The following review of information on the solid phases of the hydrogen halides obtained with different kinds of experiments

will be used subsequently for proper evaluation and possible interpretation of the results of the present investigation.

SPECIFIC HEAT[11,12,13,14]

Calorimetric measurements show three, resp. two, second order phase transitions in solid HBr, resp. HI, indicated by sharp λ-type peaks in the C_p vs. T graphs. The transitions are found to extend over temperature ranges of a few °K. The approximate transition temperatures are 89°K, 113°K, 117°K for HBr and 70°K, 125°K for HI. The change of entropy at the melting point, ΔS_m, is the same for all hydrogen halides and equals the value for the inert gases, which are known to have face-centred cubic lattices in their solid phases. At low temperatures, $C_p(T) \approx C_v(T)$ fits the T^3-law, and characteristic Debije lattice frequencies have been calculated[15].

X-RAY[16,17,18,19]

Diffraction patterns, obtained for HI, can be indexed on basis of a face-centred tetragonal cell up to at least 120°K. The highest temperature phase is face-centred cubic. No discontinuities are observed upon temperature variation through the transition regions. Density data, obtained from the lattice constants, seem to indicate a small anomaly in the temperature dependence of the volume expansion coefficient at the 125°K transition.

The results of X-ray measurements on HBr have been interpreted equivocally. The results, which have been obtained at a few temperatures only, indicate the existence of a face-centred orthorhombic crystal structure in the two lowest temperature phases.

POLARIZATION MICROSCOPE[20]

Investigation of the condensed phases of HBr and HI with the polarization microscope reveals that the high temperature solid phases of both compounds are isotropic. Lattice changes occur at

117°K for HBr and 126°K for HI, both compounds being anisotropic below these temperatures. The lower transitions do not manifest themselves, when investigated by this technique.

N.M.R.[21]

The linebroadening of nuclear magnetic resonance absorption in HBr and HI, due to spin spin interaction of the protons, has been investigated as function of temperature, in order to obtain information about the character of the phasetransitions. In a theoretical treatment of the interaction of the resonating nuclei with their environments, a "flipping time" parameter τ_c, being the average time it takes a molecule to change its orientation appreciably, is introduced and is shown to be proportional to the linewidth when τ_c is sufficiently small. From the observed absence of a rapid narrowing of the linewidth upon passage through the phasetransitions, it is concluded in view of the high frequencies of molecular rotations that none of these transitions is to be associated with the appearance of rotational degrees of freedom [22,23].

I.R.[24,25,26,27,28,29,30]

The infra-red absorption spectrum of the hydrogen halides has been investigated extensively, mainly in the lowest temperature solid phases. One of the conclusions is, that the basic structural unit in the HCl and HBr crystals is a nearly planar zigzag hydrogen-bonded chain with adjacent chains probably antiparallel, while for HI a somewhat different structure is expected. The angle between adjacent molecules is calculated to be not much different from 90°. Vibrational and librational force constants have been determined, and it is concluded that only nearest neighbour coupling is appreciable. From the ratio of the integrated line intensities of gas and crystal phases it is concluded that the molecules in the crystal have to be highly polarized. An additional phase transition for HI has been observed[28] at 25°K.

DIELECTRIC CONSTANT[31,32,33,34,35,36,37]

Investigations of the dielectric behaviour of the solid hydrogen halides, using different experimental techniques, have revealed that special precautions have to be taken with respect to sample contractions in order to obtain quantitatively reliable data. This problem is discussed in chapters 2 and 3 since it is directly relevant to the present investigation.

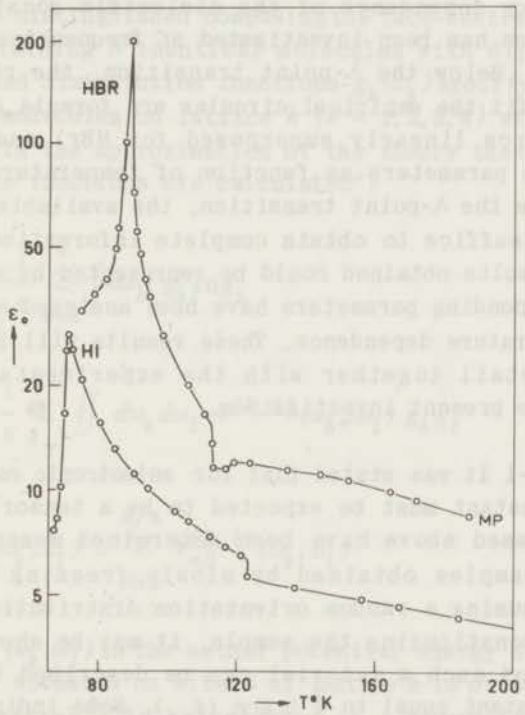

Fig. 1-1. Static dielectric constants (logarithmic scale) of hydrogen halides plotted against temperature. Data of Brown[34] for HBr and of Havriliak[36] for HI.

The temperature dependence of the static dielectric constant ϵ_o of HI and HBr (cf. fig. 1-1) measured at low frequencies, displays anomalies at the phase transitions and the transition temperatures observed closely check with those obtained from specific heat measurements. At the lower temperature transition, c.q. 70.7°K for HI and 89°K for HBr, the ϵ_o vs. T graphs show a sharp λ-type peak, while at the other transitions only a small drop in ϵ_o

occurs. The reported peak value of ϵ for HBr, measured at 20 Hz is possibly smaller than ϵ_o[34]. Small thermal hysteresis effects have been observed at the phase transitions, but it seems questionable, whether these are to be attributed to the substance under investigation. Reports about (dielectric) nonlinearity of HBr contradict each other and in the absence of any systematic investigation of this effect, definite conclusions do not seem justified.

The frequency dependence of the dielectric constant of the hydrogen halides has been investigated at frequencies between 20 Hz and 18 MHz. Below the λ-point transition, the results have been found to fit the empirical circular arc formula (one arc for HI, and two arcs linearly superposed for HBr) and values of representative parameters as function of temperature have been obtained. Above the λ-point transition, the available frequency-range did not suffice to obtain complete information. However, the limited results obtained could be represented by a semicircle and the corresponding parameters have been analysed with respect to their temperature dependence. These results will be discussed in further detail together with the experimental evidence obtained in the present investigation.

In section 1-1 it was stated that for anisotropic materials, the dielectric constant must be expected to be a tensor (ϵ_{ij}). The results discussed above have been determined measuring poly-crystalline samples obtained by slowly freezing the liquid materials. Assuming a random orientation distribution of small crystallites constituting the sample, it may be shown[38] that the response of such a material can be described by a scalar dielectric constant equal to $\frac{1}{3}$ trace (ϵ_{ij}). Some indirect support for the randomness assumption may be obtained from the fact that under special conditions violations of the assumption have been observed[34,35].

1-3. DIPOLE INTERACTION IN SOLID HYDROGEN HALIDES

A theory of phase changes due to hindered molecular rotation in crystals developed by Kirkwood[39] is applied to a face-centred orthorhombic rigid lattice of permanent point dipoles. The results

bear a remarkable similarity to Kirkwood's results obtained with a simplified interaction potential. The model does not produce the zigzag chain structure inferred from I.R. experiments, however, the results show some interesting features, in particular the importance of the ratios of the unit cell dimensions which appear as parameters in the solutions of the problem.

As in Kirkwood's treatment, four interpenetrating simple lattices are distinguished composing the face-centred orthorhombic crystal containing N identical molecules with dipole moment μ. The normalized distribution functions $g_k(\omega_k)$ specify the densities $\frac{N}{4} g_k(\omega_k)$ of molecules on lattice k ($k = 1, 2, 3, 4$) with orientation $\omega_k = \mathfrak{u}_k/\mu_k$. In the approximation of the theory the configurational thermodynamic functions are calculated*)

$$S/Nk = -\frac{1}{4} \sum_{k=1}^{4} \int d\omega_k \; g_k \ln g_k \tag{1-19}$$

$$E/N = \frac{1}{8} \sum_{k,l} \iint d\omega_k d\omega_l \; V^{(k,l)}(\omega_k, \omega_l) \; g_k g_l \tag{1-20}$$

with

$$V^{(k,l)}(\omega_k, \omega_l) = \sum_{\beta=1}^{N/4} V_{\alpha\beta}^{(k,l)}(\omega_k, \omega_l) \tag{1-21}$$

where $V_{\alpha\beta}^{(k,l)}(\omega_k, \omega_l)$ is the mutual potential energy of two molecules respectively situated on site α of lattice k in orientation ω_k and site β of lattice l in orientation ω_l. Extremalization of the free energy $F = E - TS$ with respect to the functions $g_k(\omega_k)$ leads to the integral equations

$$\ln \lambda_k \, g_k = \sum_{l=1}^{4} \int d\omega_l \; K_{kl}(\omega_k, \omega_l) g_l(\omega_l) \tag{1-22}$$

$$\lambda_k = \int d\omega_k \; \exp\left[\sum_l \int d\omega_l \; K_{kl} g_l\right] \tag{1-23}$$

where the kernels K_{kl} are equal to $-\beta V^{(k,l)}$, $(\beta = 1/kT)$.

*) In calculating the following integrals the statistical independence relation mentioned on page 23 is already implied.

For the present application, the kernels are calculated from the dipole-dipole interaction energy

$$4\pi V_{\alpha\beta}^{(k,l)}(\omega_k,\omega_l) = \frac{\boldsymbol{\mu}_k\cdot\boldsymbol{\mu}_l}{r_{\alpha\beta}^3} - 3\,\frac{(\boldsymbol{\mu}_k\cdot\mathbf{r}_{\alpha\beta})(\boldsymbol{\mu}_l\cdot\mathbf{r}_{\alpha\beta})}{r_{\alpha\beta}^5} \qquad (1\text{-}24)$$

whereas Kirkwood considered only the first term of (1-24).

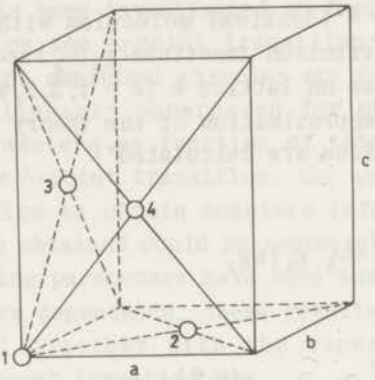

Fig. 1-2. Face-centred orthorhombic unit cell. Numbers refer to indices of interpenetrating simple lattices.

Referring to fig. 1-2 we define a coordinate system so that ω_k has components $z_k = \cos\theta_k$, $x_k = \sin\theta_k\cos\phi_k$, $y_k = \sin\theta_k\sin\phi_k$, along the **c**, **a**, **b**, principal axes respectively. Then the interaction potential (1-24) leads to the following expression for the quantities $V^{(k,l)}(\omega_k,\omega_l)$ of eq. (1-21)

$$V^{(k,l)} = A_{kl}x_kx_l + B_{kl}y_ky_l + C_{kl}z_kz_l \qquad (1\text{-}25)$$

where the coefficients A_{kl}, B_{kl}, C_{kl}, are certain lattice sums. They form matrices A, B, C, with symmetry properties required by the translational symmetry of the lattice. The bilinear form of the kernels K_{kl} now allows us to write eqs. (1-22) and (1-23) as

$$\ln\lambda_k g_k = \sum_{l=1}^{4} K_{kl}(\omega_k,\bar{\omega}_l) \qquad (1\text{-}22a)$$

$$\lambda_k = \int d\omega_k \exp\left[\sum_l K_{kl}(\omega_k, \bar{\omega}_l)\right] \tag{1-23a}$$

where

$$\bar{\omega}_l = \int d\omega_l \, \omega_l g_l(\omega_l) \tag{1-26}$$

The approximation of the method is now recognized in the relation $\overline{\boldsymbol{\mu}_i \cdot \boldsymbol{\mu}_j} = \overline{\boldsymbol{\mu}_i} \cdot \overline{\boldsymbol{\mu}_j}$ for $i \neq j$, which is equivalent to the assumption of statistical independence of the variables μ_i in the Weiss and Bragg-Williams approximations of the discrete Ising model[40]. To calculate the integrals (1-23a) we introduce vectors $\bar{\omega}_k{}^0$ with components

$$\bar{x}_k{}^0 = \sum_l A_{kl} \bar{x}_l / \bar{r}_k{}^0 \tag{1-27}$$

with corresponding expressions for $\bar{y}_k{}^0$ and $\bar{z}_k{}^0$, while

$$\bar{r}_k^0 = \left[\left(\sum_l A_{kl} \bar{x}_l\right)^2 + \left(\sum_l B_{kl} \bar{y}_l\right)^2 + \left(\sum_l C_{kl} \bar{z}_l\right)^2\right]^{1/2} \tag{1-28}$$

With the aid of these quantities, eq. (1-22a) is written

$$\ln \lambda_k g_k = -\beta \, \bar{r}_k{}^0 \cos(\omega_k, \bar{\omega}_k{}^0) \tag{1-22b}$$

The integral (1-23a) is now easily calculated as it is independent of $\bar{\omega}_k{}^0$

$$\lambda_k = \frac{4\pi \sinh \beta \, \bar{r}_k{}^0}{\beta \, \bar{r}_k{}^0} \tag{1-23b}$$

The moments $\bar{x}_k$ etc. are conveniently obtained using consistency relations of the type employed by Krieger and James[41] in a related problem

$$\bar{x}_k = \frac{\partial(\ln \lambda_k)}{\partial(-\beta \sum_l A_{kl} \bar{x}_l)} \tag{1-29}$$

$$= -L(\beta \bar{r}_k^{\,0}) \sum_l A_{kl} \bar{x}_l / \bar{r}_k^{\,0} = \rho_k^{-1} \sum_l A_{kl} \bar{x}_l \qquad (1\text{-}30)$$

where $L(x)$ is the Langevin function $\coth x - 1/x$. Eq. (1-30) defines the parameters ρ_k introduced. Clearly the result obtained implies

$$\sum_l A_{kl} \bar{x}_l / \bar{x}_k = \sum_l B_{kl} \bar{y}_l / \bar{y}_k = \sum_l C_{kl} \bar{z}_l / \bar{z}_k = \rho_k \qquad (1\text{-}31)$$

As $\bar{r}_k^{\,0} = \rho_k (\bar{x}_k^2 + \bar{y}_k^2 + \bar{z}_k^2)^{1/2} = \rho_k \bar{r}_k$, eq. (1-30) can be written

$$\bar{r}_k = - L(\beta \rho_k \bar{r}_k) \qquad (1\text{-}30a)$$

We consider only solutions of the system of equations obtained for which $\bar{r}_k$ is independent of the lattice index k. (This may be seen as a condition imposed in view of physical considerations since we did not prove that other solutions are impossible.) Then ρ_k is also independent of k because of (1-30a). Roots of ρ allowing nontrivial solutions for the system of equations (1-31) are now identified as the eigenvalues of the matrices A, B, C. The associated eigenvectors $(\bar{x}_k)$, $(\bar{y}_k)$, $(\bar{z}_k)$, cannot occur simultaneously unless all three matrices have at least one eigenvalue in common. The transition temperature corresponding to the i-th root of ρ is obtained from eq. (1-30a)

$$\beta_i \rho_i = - 3 \ , \quad T_i = - \rho_i / 3k \qquad (1\text{-}32)$$

At high temperatures only the trivial solution $\bar{r} = 0$ is possible, and all molecules are randomly oriented. At lower temperatures nonzero solutions $(\bar{r}_i)$ corresponding to the roots (ρ_i) are determined from the transcendental equation (1-30a). The thermodynamic functions become

$$\beta E/N = \beta \rho_i \bar{r}_i^{\,2}/2 \qquad (1\text{-}19a)$$

$$S/Nk = \ln \frac{4\pi \sinh \beta \rho_i \bar{r}_i}{\beta \rho_i \bar{r}_i} + \beta \rho_i \bar{r}_i^{\,2} \qquad (1\text{-}20a)$$

Differentiation of the free energy $F = E - TS$ with respect to ρ_i

at constant temperature shows that F is a monotonically increasing function of ρ_i. Hence the only solution that will be realized is the one for the largest value of $(-\rho_i)$ corresponding to the highest transition temperature. The heat capacity C_v is discontinuous at the transition temperature with a gap $\Delta C_v = 5Nk/2$ as in Kirkwood's solution.

To investigate the obtained solution more closely the eigenvalues of the matrices A, B, C, need to be evaluated. The explicit expressions for the elements are

$$4\pi A_{kl} = -\sum_{\lambda(l)}' \frac{2\mu^2}{r_\lambda^3} P_2\{\cos(\mathbf{a}, \mathbf{r}_\lambda)\} \tag{1-33}$$

where $\mathbf{r}_\lambda = (\lambda_1\mathbf{a} + \lambda_2\mathbf{b} + \lambda_3\mathbf{c})/2$ (λ_n integers) is the position vector of a lattice point, and the summation extends over all molecules at the l lattice except for the one with $\mathbf{r}_\lambda = 0$. The function $P_2(x)$ is the Legendre polynomial $(3x^2 - 1)/2$. The expressions for the elements B_{kl} and C_{kl} are obtained by cyclic permutation of the basic vectors **a**, **b**, **c**. The matrices A, B, C, defined by the coefficients (1-33) have the highly symmetrical form

$$\begin{matrix} A_1 & A_2 & A_3 & A_4 \\ A_2 & A_1 & A_4 & A_3 \\ A_3 & A_4 & A_1 & A_2 \\ A_4 & A_3 & A_2 & A_1 \end{matrix} \tag{1-34}$$

The eigenvalues and the associated eigenvectors (determined except for a constant factor) are

	$\overline{x}_1$	$\overline{x}_2$	$\overline{x}_3$	$\overline{x}_4$
$\rho_1(A) = A_1 + A_2 + A_3 + A_4$	+	+	+	+
$\rho_2(A) = A_1 + A_2 - A_3 - A_4$	+	+	-	-
$\rho_3(A) = A_1 - A_2 + A_3 - A_4$	+	-	+	-
$\rho_4(A) = A_1 - A_2 - A_3 + A_4$	+	-	-	+

(1-35)

with similar expressions for the B and C matrices. For an orthorhombic lattice the three matrices will have no common eigenvalues except possibly for very special axis ratios. The first root of (1-35) corresponds to ferroelectricity, the other three to antiferroelectric arrangement. The calculation of the lattice sums is discussed in the appendix to this section. The eigenvalues ρ_1 are dependent on the shape of the crystal, the other ones converge absolutely. The eigenvalues were calculated using the following HBr data : $a = 5.555$ Å, $b = 5.640$ Å, $c = 6.063$ Å (at 100°K[17]) and $\mu = 0.78$ D (unrationalized units). The basic vectors are taken temperature independent. The highest transition temperature, corresponding to a stable phase as discussed above, is found to be 83°K (or 102°K for nearest neighbours interaction only). Below this temperature the crystal exhibits antiferroelectricity by + + - - alignment in the direction of the b axis (note $a < b < c$).

The static admittance of the system is calculated with the aid of the formulae developed in the previous section

$$\kappa(0) = \bar{\Phi}(0)/V \tag{1-18a}$$

$$\bar{\Phi}_{xy}(0) = \beta(\overline{M_x M_y} - \overline{M}_x \overline{M}_y) \tag{1-15a}$$

where x, y, z, refer to the crystal principal axes. For the antiferroelectric solution obtained above the second term in the right hand side of (1-15a) vanishes (as in (1-15)). Further since $(\overline{x_k}) \equiv 0$ and $(\overline{z_k}) \equiv 0$, the orientational distribution functions depend on y_k only with the result that all off-diagonal elements of (1-15a) vanish. The second moment $\overline{M_y^2}$ is calculated without difficulty

$$\overline{M_y^2} = \mu^2 \sum_{\substack{k,l,\\ i,j}} \overline{y_{ki} y_{lj}} = \mu^2 N(\overline{y_k^2} - \overline{y_k}^2) \tag{1-36}$$

where the second equality results from the earlier mentioned relation $\overline{y_{ki} y_{lj}} = \overline{y_k}\,\overline{y_l}$ for $i \neq j$, combined with $\overline{M}_y{}^2 = 0$. The fluctuation of y_k is obtained from the consistency relation

$$\overline{y_k^2} - \overline{y_k}^2 = \frac{\partial^2(\ln\lambda_k)}{\partial(-\beta\sum_l B_{kl}\overline{y}_l)^2} = L'(\beta\rho\overline{y}_k) \tag{1-37}$$

where $L'(x) = \partial L/\partial x = 1 - 2L/x - L^2$ is an even function of x so that the fluctuation is independent of the lattice index. Combining the results obtained we have

$$\kappa_y(0) = \frac{\beta N\mu^2}{V} L'(\beta p\bar{y}) \qquad (1\text{-}38a)$$

The other elements are calculated in a similar way

$$\kappa_x(0) = \kappa_z(0) = \frac{\beta N\mu^2}{3V} \frac{T}{T_c} \qquad (1\text{-}38b)$$

where use has been made of the relations (1-30a) and (1-32). The results all refer to temperatures lower than T_c. Above T_c the admittance is a scalar $\kappa(0) = \beta N\mu^2/3V$, so that κ is continuous at the transition. We notice that the quantities κ_x and κ_z are temperature independent below T_c, similar to results obtained by Lax[42] and Toupin and Lax[43] in a spherical model treatment of related problems. The temperature dependence of $\kappa_y(0)$ near the transition obeys formulae derived by Kittel[44] in a phenomenological treatment of antiferroelectricity.

Calculation of the dielectric susceptibility related to κ by eq. (1-16) leads to unsatisfactory results. For a spherical specimen the factor A in (1-16) equals 1/3 and a Lorentz catastrophe occurs at 130°K, hence before the antiferroelectric transition is reached. This is due to the simplicity of the model, as the high temperature expression $\kappa = \beta N\mu^2/3V$ is a direct result of the statistical independence relation $\overline{\boldsymbol{\mu}_i \cdot \boldsymbol{\mu}_j} = \overline{\boldsymbol{\mu}_i} \cdot \overline{\boldsymbol{\mu}_j}$ for $i \neq j$.

A difficulty in connection with the boundary conditions of the model should be mentioned. The translational symmetry implied clearly requires cyclic boundary conditions. However, the first eigenvalue in (1-35) is a conditionally convergent lattice sum, as discussed in the appendix. Hence a specific shape is required to rule out ferroelectricity. The conditions can be reconciliated by introduction of a suitable convergence factor[42]. The difficulty does not arise when only nearest neighbour interactions are considered.

APPENDIX TO SECTION 1-3

The evaluation of the lattice sums determining the eigenvalues ρ_i of (1-35) is performed with aid of a method due to de Wette[45]. The roots ρ_i corresponding to antiferroelectric arrangement are absolutely convergent lattice sums. They can be written, using (1-33)

$$\rho_2(A) = A_1 + A_2 - A_3 - A_4$$

$$= -\frac{\mu^2}{4\pi} \sum_{\lambda}{}' \{(-1)^{\lambda_1 + \lambda_2} + (-1)^{\lambda_3}\} r_\lambda^{-3} P_2\{\cos(\mathbf{a}, \mathbf{r}_\lambda)\} \quad (1\text{-}39)$$

where $2\mathbf{r}_\lambda = \lambda_1 \mathbf{a} + \lambda_2 \mathbf{b} + \lambda_3 \mathbf{c}$ (λ_n integers). The roots $\rho_3(A)$, $\rho_4(A)$, $\rho_2(B)$, etc. are obtained by cyclic permutations. First the position vector is rescaled by introduction of a vector $\mathbf{s}_\lambda = 2\mathbf{r}_\lambda/b$. Eq. (1-39) now becomes

$$-\frac{4\pi}{\mu^2} \rho_2(A) \frac{b^3}{8} = S_2'(A) \quad (1\text{-}40)$$

$$S_2'(A) = \sum_{\lambda}{}' \{(-1)^{\lambda_1 + \lambda_2} + (-1)^{\lambda_3}\} s_\lambda^{-3} P_2\{\cos(\mathbf{a}, \mathbf{s}_\lambda)\}$$

Next the terms are multiplied with an auxiliary function $\{\Gamma(\frac{5}{2}, \pi s_\lambda^2) + \gamma(\frac{5}{2}, \pi s_\lambda^2)\} / \Gamma(\frac{5}{2}) = 1$, where $\Gamma(n,x)$ and $\gamma(n,x)$ are incomplete gamma functions, and $S_2'(A)$ is split in two sums $S_{2d}'(A)$ and $S_{2r}'(A)$ referring to the two terms in the auxiliary function. $S_{2d}'(A)$ is easily calculated due to the presence of the rapidly converging function $\Gamma(\frac{5}{2}, \pi s^2)$. The second sum is written as a threedimensional integral over $\mathbf{s}$ space

$$S_{2r}' = \int d\mathbf{s}\, F_1 F_2 \quad (1\text{-}41)$$

with

$$F_1 = \sum_{\lambda} \{e^{2\pi i \mathbf{h}_1 \cdot \mathbf{s}} + e^{2\pi i \mathbf{h}_2 \cdot \mathbf{s}}\} \delta(\mathbf{s} - \mathbf{s}_\lambda)$$

$$F_2 = \frac{\gamma(\frac{5}{2}, \pi s^2)}{\Gamma(\frac{5}{2}) s^3} P_2\{\cos(\mathbf{a}, \mathbf{s})\}$$

where $2\,\mathbf{h}_1 = (\mathbf{a}b/a^2 + \mathbf{b}/b)$ and $2\,\mathbf{h}_2 = \mathbf{c}b/c^2$ are vectors in reciprocal space. The prime in the sum F_1 has been omitted as the term with $\lambda = 0$ vanishes. The integral (1-41) may now be converted to an integral of $\hat{F}_1\hat{F}_2$ ($\hat{}$ indicates threedimensional Fourier transform) over reciprocal space and can be written as a sum over the reciprocal lattice. Straightforward application of de Wette's formulae gives the result

$$S'_{2r} = -\frac{4\pi}{3v}\left[\sum_{\lambda} e^{-\pi|\mathbf{h}_\lambda - \mathbf{h}_1|^2} P_2\{\cos(\mathbf{a}, \mathbf{h}_\lambda - \mathbf{h}_1)\}\right.$$

$$\left. + \sum_{\lambda} e^{-\pi|\mathbf{h}_\lambda - \mathbf{h}_2|^2} P_2\{\cos(\mathbf{a}, \mathbf{h}_\lambda - \mathbf{h}_2)\}\right] \qquad (1\text{-}42)$$

where $v = ac/b^2$. The sum obtained also converges rapidly and the eigenvalues can be evaluated to any degree of accuracy.

The roots ρ_1 corresponding to ferroelectric arrangement are conditionally convergent lattice sums. When these sums are treated by the method discussed above the main contribution is found to result from one term in the reciprocal lattice sum

$$-\frac{4\pi}{\mu^2}\rho_1(A)\,\frac{b^3}{8} \approx -\frac{4\pi}{3v}\lim_{\mathbf{h}\to 0} e^{-\pi h^2} P_2\{\cos(\mathbf{a}, \mathbf{h})\} \qquad (1\text{-}43)$$

The limit expression in (1-43) can have any value between - 1/2 and 1 depending on the shape of the crystal. The explicit relation between the order of summation in ordinary space and the way of approaching the origin in reciprocal space is not known[45]. Comparison with the antiferroelectric roots using the numerical HBr data of section 1-3 shows that the antiferroelectric transition discussed is the stable one, provided the shape of the crystal can be chosen (ellipsoid not differing much from spherical shape) so that $\lim_{\mathbf{h}\to 0} \cos^2(\mathbf{a}, \mathbf{h}) > 0.12$ for all three direction cosines.

REFERENCES

(1) L.D. Landau and E.M. Lifshitz, *The classical Theory of Fields*, (Addison-Wesley Publishing Company, Inc., Reading, Massachusetts, 1962).

(2) K.S. Cole and R.H. Cole, J. Chem. Phys. **9**, 341 (1941).

(3) D.W. Davidson and R.H. Cole, J. Chem. Phys. **19**, 1484 (1951).

(4) P. Debije, *Polar Molecules*, (Dover Publications, Inc., New York).

(5) P. Mazur, Advan. Chem. Phys. **1**, 309 (1958).

(6) R. Kubo, J. Phys. Soc. Japan **12**, 570 (1957).

(7) S.H. Glarum, J. Chem. Phys. **33**, 1371 (1960).

(8) R.H. Cole, J. Chem. Phys. **42**, 637 (1965).

(9) E. Braun and P. Mazur, (unpublished).

(10) W.F. Brown Jr. in *Handbuch der Physik*, edited by S. Flügge (Springer Verlag, Berlin, 1956) Band XVII.

(11) A. Eucken and E. Karwat, Z. Physik. Chem. **112**, 467 (1924).

(12) W.F. Giauque and R. Wiebe, J. Am. Chem. Soc. **50**, 2193 (1928).

(13) W.F. Giauque and R. Wiebe, J. Am. Chem. Soc. **51**, 1441 (1929).

(14) A. Eucken and W. Güttner, Gött. Nachr., Math. Phys. Kl. Fachgr. II **2**, 167 (1936).

(15) E.A. Moelwyn-Hughes, *Physical Chemistry*, (Cambridge University Press, London, 1940) p. 132.

(16) B. Ruhemann and F. Simon, Z. Physik. Chem. **15B**, 389 (1931).

(17) G. Natta, Nature **126**, 97 (1930); Nature **127**, 235 (1931); Gazz. Chim. Ital. **63**, 425 (1933).

(18) *Crystal Data*, edited by J.D.H. Donney *et al.* (American Crystallographic Association, 1963) pp. 497, 584.

(19) F.A. Maurer, C.J. Keffer, R.B. Reeves, and D.W. Robinson, J. Chem. Phys. **43**, 1465 (1965).

(20) A. Kruis and R. Kaischew, Z. Physik. Chem. **B41**, 427 (1939).

(21) N.A. Alpert, Phys. Rev. **75**, 398 (1949).

(22) L. Pauling, Phys. Rev. **36**, 430 (1930).

(23) R.H. Fowler, Proc. Roy. Soc. London **A149**, 1 (1935).

(24) G.L. Hiebert and D.F. Hornig, J. Chem. Phys. **20**, 918 (1952).

(25) D.F. Hornig and W.E. Osberg, J. Chem. Phys. **23**, 662 (1955).

(26) E.D. Becker and G.C. Pimentel, J. Chem. Phys. **25**, 224 (1956).
(27) D.F. Hornig and G.L. Hiebert, J. Chem. Phys. **27**, 752 (1957).
(28) G.L. Hiebert and D.F. Hornig, J. Chem. Phys. **26**, 1762 (1957).
(29) H.B. Friedrich and W.B. Person, J. Chem. Phys. **39**, 811 (1963).
(30) R. Savoie and A. Anderson, J. Chem. Phys. **44**, 548 (1966).
(31) C.P. Smyth and C.S. Hitchcock, J. Am. Chem. Soc. **55**, 1830 (1933).
(32) J.G. Powles, Nature **165**, 686 (1950); Compt. Rend. **230**, 836 (1950); J. Phys. Radium **13**, 121 (1952).
(33) C.S. Philips, J. Phys. Radium **13**, 216 (1952).
(34) N.L. Brown, Ph.D. thesis, Brown University, (1952).
(35) N.L. Brown and R.H. Cole, J. Chem. Phys. **21**, 1920 (1953).
(36) S. Havriliak, Jr., Ph.D. thesis, Brown University, (1958).
(37) R.H. Cole and S. Havriliak, Jr., Discussions Faraday Soc. **23**, 31 (1957).
(38) J.F. Nye, *Physical Properties of Crystals*, (Clarendon Press, Oxford, England, 1957) p. 66.
(39) J.G. Kirkwood, J. Chem. Phys. **8**, 205 (1940).
(40) R.H. Brout, *Phase Transitions*, (W.A. Benjamin, Inc., New York, 1965).
(41) T.J. Krieger and H.M. James, J. Chem. Phys. **22**, 796 (1954).
(42) M. Lax, J. Chem. Phys. **20**, 1351 (1952).
(43) R.A. Toupin and M. Lax, J. Chem. Phys. **27**, 458 (1957).
(44) C. Kittel, Phys. Rev. **82**, 729 (1951).
(45) F.W. de Wette, Dissertatie, R.U. Leiden, (1959) p. 19; Physica **23**, 309 (1957); Physica **24**, 1105 (1958).

CHAPTER 2

MEASURING TECHNIQUE

Description of electrical apparatus in terms of lumped circuit theory becomes inadequate as soon as the dimensions of the various parts of the apparatus amount to an appreciable fraction of the wavelengths corresponding to the frequencies involved. On the other hand the electromagnetic theory of propagation of waves, as governed by Maxwell's equations, is only useful if the geometry of the relevant parts of the apparatus allows us to find simple solutions for these equations. The frequencies employed in the present investigation, between 5 MHz and 250 MHz, necessitate the use of both concepts to arrive at a satisfactory description of the electrical behaviour of the various parts of the equipment. So, the measuring instrument will be treated by lumped circuit theory, while the cell that is to contain the unknown material and the connection leads between the cell and the instrument will be analyzed in terms of transmission line theory.

2-1. BOONTON RX METER

The RX Meter [1] Type 250-A measures admittance as parallel capacitance and conductance in the frequency range from 0.5 to 250 MHz.

In order to investigate how the measured admittance is influenced by the residual circuit parameters suggested by the manufacturers of the instrument, we derive the relation between the unknown admittance and the circuit elements. Referring to fig. 2-1, balance of the bridge circuit as indicated by minimum deflection of the null indicator N, is obtained for

$$Y_1 Y_3 = Y_2 Y_4 \qquad (2\text{-}1)$$

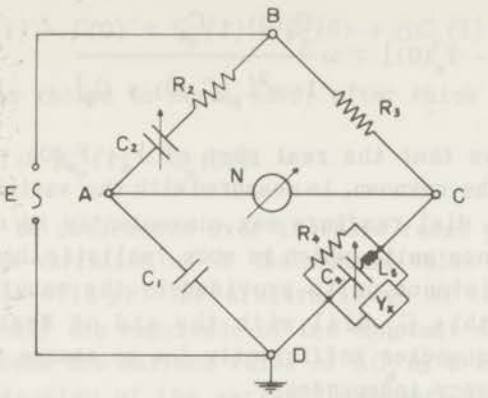

Fig. 2-1. Schematic bridge circuit.

Writing out the components

$$Y_1 = i\omega C_1 \quad , \quad Y_2 = (R_2 + \frac{1}{i\omega C_2})^{-1}$$

$$Y_3 = \frac{1}{R_3} \quad , \quad Y_4 = \frac{1}{R_4} + Y_x + \frac{i\omega C_4}{1-\omega^2 L_s C_4} \tag{2-2}$$

and substituting into (2-1) gives the condition

$$\frac{i\omega C_1}{R_3}(R_2 + \frac{1}{i\omega C_2}) = \frac{1}{R_4} + \frac{i\omega C_4}{1-\omega^2 L_s C_4} + Y_x \tag{2-3}$$

This equation shows how the two variable capacitors C_2 and C_4 are used to compensate for, respectively, the real and imaginary part of the unknown admittance Y_x. In order to obtain Y_x in terms of dial readings we subtract from (2-3) the corresponding equation for Y_x (0), by which we indicate a reference termination (e.g. nothing connected to the RX Meter binding posts). Separating the real and imaginary parts of the resulting equation, we obtain

$$\mathcal{R}\,[Y_x - Y_x(0)] = \frac{C_1}{R_3}\left[\frac{1}{C_2} - \frac{1}{C_2(0)}\right] \tag{2-4}$$

$$\mathfrak{I}\,[Y_x - Y_x(0)] = \omega \frac{C_4(0) - C_4}{1 - \omega^2 L_s [C_4(0) + C_4]} \qquad (2\text{-}5)$$

Eq. (2-4) shows that the real part of $Y_x - Y_x(0)$, the parallel conductance of the unknown, is measured with the variable capacitor C_2. Hence the C_2 dial readings may conveniently be calibrated in terms of conductance units, which is more realistic than calibration in terms of resistance units provided by the manufacturers. We re-calibrated this C_2 dial with the aid of Weston standard resistors at frequencies sufficiently low to assure their resistance to be frequency independent.

From eq. (2-5) it is seen that for sufficiently low frequencies the parallel capacitance of the unknown is obtained directly from readings of the variable capacitor C_4. Positive capacitance readings made on the yellow portion of the C_p dial marked "+" are related to C_4 values according to: $C_4 = A - C_p$ with A approximately equal to 40 pF. So, measuring purely capacitative components we have according to (2-5) for low frequencies

$$C_x(2) - C_x(1) = C_4(1) - C_4(2) = C_p(2) - C_p(1) \qquad (2\text{-}6)$$

The C_p dial, however, was found to have a more or less systematic deviation, which can be represented by

$$(C_p)_{corr} = C_p + \Delta C_p$$

giving instead of (2-6)

$$C_x(2) - C_x(1) = C_p(2) - C_p(1) + \Delta C_p(2) - \Delta C_p(1) \qquad (2\text{-}7)$$

A calibration graph of ΔC_p versus C_p is obtained by the following procedure. We measure a linearly variable capacitor, the capacitance of which is represented by

$$C(l) = D + Bl \qquad (2\text{-}8)$$

with B accurately known from the geometry of the capacitor and l a continuously variable length parameter to be measured with a suitable micrometer. According to (2-7) we have

$$Bl = C(l) - C(0) = C_p(l) - C_p(0) + \Delta C_p(l) - \Delta C_p(0) \quad (2\text{-}9)$$

Here $\Delta C_p(0)$ is chosen to equal zero, after which

$$\Delta C_p = Bl - [C_p(l) - C_p(0)] \quad (2\text{-}10)$$

Thus ΔC_p may be determined over te whole range of C_p of interest by appropriate variation of l. The maximum value of the correction so obtained is 0.15 pF. The arbitrariness of the choice $\Delta C_p(0) = 0$ affects only the magnitude of the constant A, the inaccuracy of which exceeds the maximum value of ΔC_p by a factor 10.

The determination of the series inductance L_s of C_4 involves use of transmission lines and will therefore be discussed at the end of section 2-2 (page 43). The value obtained for L_s is 0.89×10^{-9} H.

All measured conductances and capacitances were corrected with the aid of the above discussed correction graphs to obtain the data presented in this thesis. At frequencies higher than 40 MHz, further corrections were made for L_s.

At this point we want to mention that some investigators [2,3] have considered a stray reactive component parallel to R_3 (cf. fig. 2-1). Inspection of eq. (2-3) reveals that this results in an additional term in eq. (2-5), which makes the measured capacitance a function of the unknown conductance. If the reactive component is an inductance parallel to R_3, we also find the measured conductance to be a function of frequency. As evaluation of this component cannot be done without making assumptions about the test elements to be used (e.g. ionic solutions), we consider it undesirable to take these possible effects into account. Their effect is in any case important only for much larger conductances than were involved in the present measurements.

2-2. COUPLING LINES

From fig. 2-1 we see that the unknown admittance Y_x, which we have left unspecified until now, is the input admittance of the branch containing the unknown component, as seen by the measuring circuit at the branchpoints across the variable capacitor C_4. So, any connection leads that necessarily have to be used to connect

the terminating component of interest Y_t (e.g. the cell) to the measuring circuit must be included in Y_x. The situation is pictured in fig. 2-2, where the connecting leads are represented by a four terminal network N. The method used to meet the difficulties connected with the use of coupling networks was originally developed by Cole[4], and parts of the following analysis are based on his work.

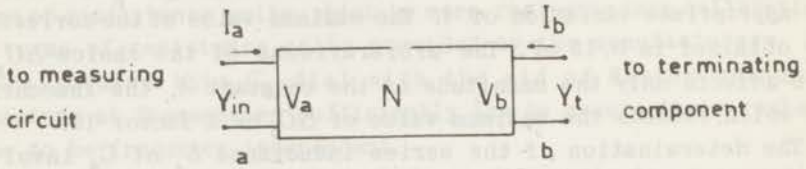

Fig. 2-2. Connecting leads represented by four terminal coupling network.

Assuming linear passive elements only in N, the voltages and currents, as indicated, obey linear relations

$$I_a = AV_a + BV_b$$
$$I_b = CV_a + DV_b \qquad (2\text{-}11)$$

with the additional condition $B = C$, according to the reciprocity theorem, provided there are no unidirectional elements in N. Introducing the short circuit impedances z_a, z_b and the open circuit admittances y_a, y_b as defined by

$$z_a = \frac{V_a}{I_a} \quad \text{if } V_b = 0, \qquad y_a = \frac{I_a}{V_a} \quad \text{if } I_b = 0$$
$$z_b = \frac{V_b}{I_b} \quad \text{if } V_a = 0, \qquad y_b = \frac{I_b}{V_b} \quad \text{if } I_a = 0 \qquad (2\text{-}12)$$

to replace the coefficients A, B, C, D, and solving for the input admittance $Y_{in} = I_a/V_a$ at a when the end b is terminated by an admittance $Y_t = -I_b/V_b$, we obtain

$$Y_{in}(a) = \frac{(\frac{z_b}{z_a})Y_t + y_a}{1 + z_b Y_t} \qquad (2\text{-}13)$$

together with the necessary condition

$$y_a z_a = y_b z_b \qquad (2\text{-}14)$$

In order to use the general admittance transformation expressed by eq. (2-13) for evaluation of Y_t from Y_{in} measurements, knowledge is required of all three quantities characterising N.

In the following we study the special case in which N may be represented by a uniform transmission line. Next we discuss whether this condition is satisfied in the practical situation at hand, and consider how much small deviations from uniformity affect the obtained results.

Voltage and current in a two-conductor transmission line with series resistance r, series inductance L, shunt capacitance C and shunt conductance g, all per unit length, obey partial differential equations

$$L\frac{\partial I}{\partial t} + rI = -\frac{\partial V}{\partial x}, \quad C\frac{\partial V}{\partial t} + gV = -\frac{\partial I}{\partial x} \qquad (2\text{-}15)$$

For sinusoidal time dependence these equations reduce to

$$\frac{dV}{dx} = -ZI \quad , \quad \frac{dI}{dx} = -YV \qquad (2\text{-}16)$$

where we have introduced the series impedance $Z = r + i\omega L$ and the shunt admittance $Y = g + i\omega C$, both per unit length. For a uniform line the line parameters are obviously constant, and by differentiating (2-16) with respect to x we obtain two homogeneous second order equations

$$\frac{d^2V}{dx^2} = YZV \quad , \quad \frac{d^2I}{dx^2} = YZI \qquad (2\text{-}17)$$

with the solutions, taking account of (2-16)

$$V(x) = Ae^{\gamma x} + Be^{-\gamma x} \quad , \quad I(x) = \frac{-1}{Z_o}(Ae^{\gamma x} - Be^{-\gamma x}) \tag{2-18}$$

where

$$\gamma = \sqrt{YZ} \quad \text{and} \quad , \quad Z_o = \sqrt{\frac{Z}{Y}}$$

Introducing, as before, the quantities y_o and z_s (as a uniform line is symmetrical, $y_a = y_b = y_o$ and $z_a = z_b = z_s$) we find for a line of length l

$$y_o = \frac{1}{Z_o} \tanh\gamma l \quad , \quad z_s = Z_o \tanh\gamma l \tag{2-19}$$

The input admittance at $x = 0$, when the line is terminated at $x = l$ with a load Y_t, is in agreement with (2-13) found to be

$$Y_{in} = \frac{Y_t + y_o}{1 + z_s Y_t} \tag{2-20}$$

For an arbitrary line length l the two quantities y_o and z_s will, in general, be complex and may amount to large values. This is undesirable for the calculation of Y_t from Y_{in}. Therefore we look for special lengths of l so that y_o and z_s both become small and preferably not complex.

SHORT LINES

If l is small enough to make $\gamma l \ll 1$, we may in (2-19) replace tanh by the first term of the series expansion, leading to the simplifications

$$y_o = (g + i\omega C) l \frac{\tanh\gamma l}{\gamma l} = (g + i\omega C) l$$
$$z_s = (r + i\omega L) l \tag{2-21}$$

For short leads, both the leakage conductance gl and series resistance rl will be negligible, and the transformation (2-20) reduces to

$$Y_{in} = \frac{Y_t + i\omega Cl}{1 + i\omega Ll Y_t} \qquad (2\text{-}22)$$

The standard expressions for the line parameters give for a 50 ohm line

$$C = 67 \text{ pF/m} \quad , \quad L = 0.166 \ \mu\text{H/m}$$

The present case is realized, for example, when the Boonton RX Meter is used to measure a component that is connected directly to the binding posts on top of the instrument. According to the manual the leads inside the instrument towards the measuring circuit proper are roughly equivalent to two inches of 50 ohm line, corresponding to an inductance of 0.008 μH. This introduces a correction of 30% for a capacitor of 20 pF measured at 250 MHz with an inaccuracy of about 5%. (The value of 0.003 μH for the inductance of the binding posts, as given by the manual, is in disagreement with the above obtained result, and would give a smaller correction. At the same time the discrepancy demonstrates the uncertainty in the value of this inductance).

The requirement that the connection leads are kept as short as possible becomes rather inconvenient if one wishes to make measurements of a component in a low temperature thermostat. Therefore the solution of resonant length lines was used, to be discussed next.

RESONANT LENGTH LINES

In order to demonstrate the effectiveness of this solution, we assume that the leakage conductance and the series resistance of the line may be neglected. The propagation constant γ is then purely imaginary and both voltage and current are represented by plane waves travelling in both directions

$$V = Ae^{i\omega t + \gamma x} + Be^{i\omega t - \gamma x}$$
$$= Ae^{i\omega(t + x\sqrt{LC})} + Be^{i\omega(t - x\sqrt{LC})} \qquad (2\text{-}23)$$

with a phase velocity

$$v = \frac{\omega\lambda}{2\pi} = \frac{1}{\sqrt{LC}} \qquad (2\text{-}24)$$

For air line, $v = c$, the velocity of light, and $\lambda = \lambda_o$, the free space wavelength, while for a dielectric filled line $\lambda = \lambda_o/\sqrt{\epsilon}$. From eq. (2-19) it is seen that both y_o and z_s will equal zero for

$$\tanh\gamma l = i \tan\omega l\sqrt{LC} = 0$$
$$\omega l_n\sqrt{LC} = n\pi \qquad l_n = \frac{n\pi}{\omega\sqrt{LC}} = \frac{n}{2}\lambda \qquad (2\text{-}25)$$

where n is an integer, while (2-20) reduces to

$$Y_{in} = Y_t$$

showing that for this condition the admittance transformation reduces to a simple equality. Since no corrections have to be applied, this solution is very attractive as long as the necessary line lengths do not become inconveniently large.

The assumption that the leakage conductance may be neglected is justifiable for commercial cables of good quality. Resistive losses, however, will always be present and their influence has to be taken into consideration. For this purpose, we expand Z_o and $\tanh\gamma l_n$ in powers of r and study the effects of additional terms

$$Z_o = \sqrt{\frac{r + i\omega L}{i\omega C}} = R_o + \frac{r}{2i\omega CR_o} + \ldots \qquad (2\text{-}26)$$

$$\tanh\gamma l_n = \tanh l_n\sqrt{i\omega C(r + i\omega L)}$$
$$= \frac{rl_n}{2R_o} + i\frac{r^2 l_n}{8\omega CR_o^3} \qquad (2\text{-}27)$$

where $R_o = \sqrt{L/C}$. Using these approximations we find

$$y_o = \frac{r l_n}{2R_o^2} + i \frac{3 r^2 l_n}{8 \omega C R_o^4} \tag{2-28}$$

$$z_s = \frac{r l_n}{2} - i \frac{r^2 l_n}{8 \omega C R_o^2} \tag{2-29}$$

The imaginary terms are found to be negligible for frequencies higher than 10 MHz and the transformation for the resonant lossy line section becomes

$$Y_{in} = \frac{Y_t + \dfrac{r_s}{2R_o^2}}{1 + \dfrac{r_s}{2} Y_t} \tag{2-30}$$

where r_s is the resistance of the whole line. (We note that, in the approximation carried through here, the transformation becomes an identity when the line is terminated by a pure resistor of magnitude $R_o = \sqrt{L/C}$.)

The established result is based on the assumption that the connection leads may be represented by a uniform transmission line. In practice the line is composed of several pieces of 50 ohm line and there will be, of course, reflections along the line due to connectors, switches, supporting beads, bends in the line etc. However, care was taken while constructing the lines to satisfy the condition of symmetry as much as possible, so that we may assume that $z_a = z_b = z_s$ in (2-13). The nonuniformity then may upset eq. (2-30) in that it proves impossible to find a line length l_n such that both z_s and y_o become real. This is easily checked experimentally by measuring a pure resistance. For most lines eq. (2-30) was found to hold, while deviating behaviour in other ones could be compensated for.[4]

Summarizing the foregoing treatment we conclude that in order to use the resonant length method we need a set of symmetrical lines with lengths corresponding to the frequencies of interest according to $l_n = n\lambda/2$. Then the effect of a line at its resonant frequency is represented by the admittance transformation (2-30), where R_o, the characteristic impedance, is a pure resistance and r_s is an empirical quantity representing the resistive losses along the line. For all lines used, $R_o = 50$ ohm and determined values of r_s did not exceed 2 ohm.

Fig. 2-3 shows the schematic line system as it was constructed, to be compared with the network of fig. 2-2. Symmetry is preserved around the midpoint between the two switches A and B, and the two pieces B_1 and B_2 are electrically identical. The practical procedure of measuring Y_t consists of the following steps:

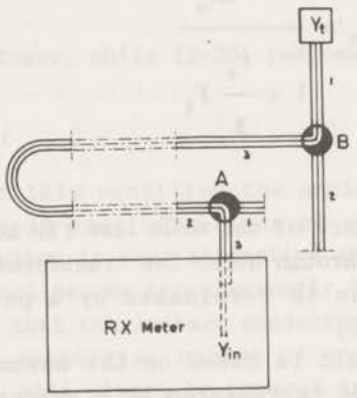

Fig. 2-3. Schematic line system. A and B are coaxial switches. Length of dashed section between A and B may be varied.

1. We connect between A and B a coaxial line such that the whole line length between Y_{in} and Y_t corresponds to the desired frequency according to (2-25), and select a frequency close to the expected resonating value.
2. We measure a pure 50 ohm resistor at end A_1. This gives the "zero capacitance" reading on the C_p dial for the chosen setting of the C_p-balance control capacitor. (cf. eq. (2-22) where $L/C = R_o^2$).

3. We then adjust either the frequency or the line length until the line up to the open circuited end B_2 measures the same "zero capacitance". This ensures that y_o is a real quantity, as is z_s, according to the discussion above.

4. In order to find r_s for the chosen line we measure the conductance difference between the open ends A_1 and B_2, which is equal to $r_s/2R_o^2$. If desirable, the resistance of the first piece of line up to A_1 may be estimated by measuring the piece B_3 to B_2 and using symmetry considerations.

5. After these preliminaries we measure Y_t, located as indicated in the picture, and y_o, i.e. the open circuited end B_2. Then Y_t is obtained from eqs. (2-4) and (2-5) where $Y_x - Y_x(0)$ is related to Y_t by

$$Y_x - Y_x(0) = Y_{in} - y_o$$

$$= \frac{Y_t + \frac{r_s}{2R_o^2}}{1 + \frac{r_s}{2} Y_t} - \frac{r_s}{2R_o^2} = \frac{Y_t}{1 + \frac{r_s}{2} Y_t} \qquad (2\text{-}31)$$

The main difficulty in this procedure lies in step 2 in deciding whether a given 50 ohm resistor is satisfactorily purely resistive. Inspection of the relevant formulae reveals that possible improper adjustment, due to some reactance in the 50 ohm resistor, results in a small inductance term, to be added to $r_s/2$ in eq. (2-31).

All measurements leading to the data in this thesis were made with the aid of the above discussed scheme except the ones at 4.4 MHz, where use was made of a delay line[4].

Finally we discuss the determination of the residual inductance L_s in series with the capacitor C_4 in the Boonton RX Meter bridge circuit. Measuring the difference of two capacitors we have according to eq. (2-5)

$$C_{x1} - C_{x2} = \frac{C_{42} - C_{41}}{1 - \omega^2 L_s (C_{42} + C_{41})} \qquad (2\text{-}32)$$

with C_4 = 40 pF - C_p. Here and in the following discussion C_x is an apparent frequency dependent capacitance to be distinguished from the zero frequency capacitance. With the aid of the C_p balance control, a small variable capacitor parallel to C_4, we may vary a particular balancing C_4 setting over approximately 4 pF. This allows us to vary the values of $(C_{42} - C_{41})$ and $(C_{42} + C_{41})$ while keeping the right hand side of eq. (2-32) constant. From a plot of $(C_{42} - C_{41})$ versus $(C_{41} + C_{41})$ the quantities $(C_{x1} - C_{x2})$ and $\omega^2 L_s$ may be evaluated from the intercept and the slope of the straight line. So far this determination of L_s is rather crude, since individual balancing C_4 settings can be varied only over 4 pF. An appreciable improvement is obtained by the following procedure. Let the terminations C_{x1} and C_{x2} refer to two open transmission lines of variable length. Then, at a particular high frequency, the imaginary parts of their input admittances (corresponding to C_x) may, according to (2-19), have any value between $-\infty$ and $+\infty$ depending on their length, and therefore they may serve as variable capacitors. We now distinguish the following steps in the experimental procedure:

1. At a particular high frequency, the C_p balance control is set on minimum capacity position, and C_{x1} and C_{x2} adjusted in such a way that the corresponding C_4 readings are at the high end of the C_4 scale with a difference of 50 pF, for example, (e.g. C_{41} = 140 pF, C_{42} = 90 pF, corresponding to C_{p1} = -100 pF, C_{p2} = -50 pF).
2. We change C_p balance control to maximum capacity position and measure again. This gives C_4 or C_p values shifted over 4 pF (C_{41} = 136 pF, C_{42} = 86 pF).
3. We change C_p balance control back to minimum position and adjust C_{x1} and C_{x2} such that the balancing C_{41} and C_{42} values are exactly the same as those observed in step 2. This ensures that the left hand side of equation (2-32) still has the same original (undetermined) value.
4. From here we proceed as under step 2. etc.

In this way an extended series of $(C_{42} - C_{41})$ and $(C_{42} + C_{41})$ values is obtained, from which again L_s is determined as indicated above. Determined L_s values at 150 MHz and 225 MHz agree within 5%, and the value used in this investigation is 0.89×10^{-9}H. (Again a discrepancy with the value of the instruction manual is found. Comparing this with the disagreement in the value of the inductance of the binding posts already mentioned, and considering

that these two different inductances cause deviations in opposite directions, we conclude that the values given in the instruction manual are to be considered "practical" values).

2-3. DIELECTRIC CELL

After the foregoing discussions, it remains to be shown how the dielectric properties of the material of investigation, as expressed by $\epsilon = \epsilon' - i\epsilon''$, are evaluated from Y_t. At sufficiently low frequencies Y_t is the admittance of a capacitor of geometrical capacitance C_o containing a sample material in between the two electrodes, and the desired relation is given by

$$Y_t = i\omega\epsilon C_o = \omega\epsilon'' C_o + i\omega\epsilon' C_o \qquad (2\text{-}33)$$

if precautions are taken to assure that this formula is valid.

Eq. (2-33) requires that all space between the two electrodes is homogeneously filled with sample material, a condition that will generally present few difficulties as long as gases or liquids are measured. A solid sample, however, will not always occupy the whole available volume of a capacitor of rigid construction upon temperature variation, due to a difference in thermal expansion coefficient of metals and dielectrics. A possible way of overcoming this difficulty experimentally is by use of a parallel plate capacitor, in which pressure can be applied to one non-fixed electrode after insertion of the dielectric, such that this electrode follows at all times any expansion or contraction of the sample. A variation of this method[5,6,7] is obtained by containing electrodes and sample in some "squeeze" device with sufficiently large expansion coefficient and proper elasticity. Only if precautions of this kind to prevent voids lying parallel to the electrodes are taken, can eq. (2-33) be used as a good approximation at all temperatures. We notice, however, that in this case $C_o(T)$ will be a function of the thermal expansion coefficient of the dielectric.

The frequencies involved and the measuring instrument used for this investigation make a capacitor of other than coaxial construction undesirable because of the increasing complexity of inductance effects at higher frequencies. Furthermore, the

properties of the hydrogen halides also impose restrictions on our choice of cell construction: the sample has to enter the cell as a gas or a liquid and so it must be possible to include the cell in a closed distilling system in order to obtain a sample of the anhydrous compound. We decided that construction of a cell that compensated for the problem stated above was not satisfactorily realizable.

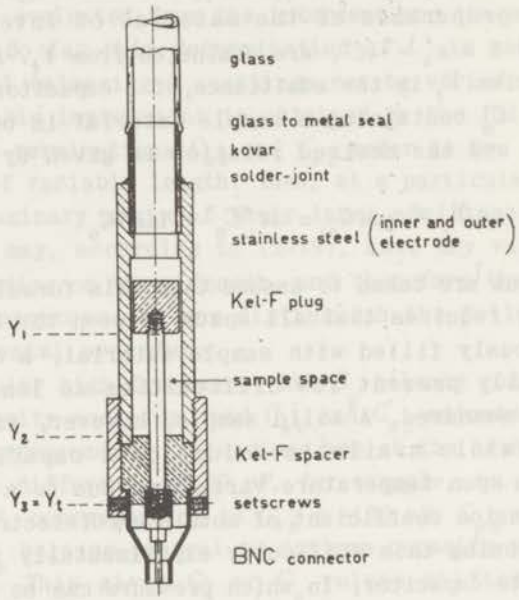

Fig. 2-4. Coaxial cell for dielectric measurements. The upper Kel-F plug has a diameter smaller than the surrounding outer electrode, allowing a liquid to pass down.

The finally adopted construction, as pictured in fig. 2-4, consists of a pair of coaxial conductors made to fit a commercial adaptor in order to allow for connection to the transmission line system. At the top, the outer conductor fits a commercial metal to glass seal, allowing for connection to a glass distilling apparatus for sample transfer purposes. The inner electrode is kept in place by a Kel-F spacer (the lower one shown in the drawing) and provision is made for use of a pressure sensitive metal to fluorocarbon plastic adhesive, such that the bottom of

the cell may be satisfactorily sealed off. The upper Kel-F plug fits the outer conductor loosely and has either groves or holes to allow a liquid to pass down, but, from an electrical point of view, is supposed to occupy the indicated region completely. The whole construction is easily taken apart for cleaning purposes and also makes it possible to measure the distance l_o between the two Kel-F spacers, while assembling or disassembling the cell.

As discussed above, a cell of this construction will not at all temperatures be homogeneously filled with the solid sample and eq. (2-33) is not applicable. We will proceed to derive a modification of eq. (2-33) to account for incomplete filling by first studying the electrical properties of the completely homogeneously filled cell, and next investigating the effects of sample contraction.

Referring to fig. 2-4. we may formally distinguish three short sections of coaxial line that contribute to Y_t, as indicated. We label by Y_1, Y_2, $Y_3 = Y_t$ the input admittances of respectively section 1, section 1+2, section 1+2+3. We assume that Y_1 is only dependent on the geometry of the two conductors and of the dielectric constant of Kel-F, but independent of the presence of any material present above the plug. (This assumption is justified when the plug extends far enough above the inner conductor.) Since Kel-F shows negligible dispersion in the frequency region of interest and the length of this section is short, Y_1 will at all considered frequencies be represented by

$$Y_1 = i\omega\Delta C_1 \tag{2-34}$$

Calculating Y_2 with the aid of the transformation formulae derived in section 2-2 we obtain

$$Y_2 = \frac{i\omega\Delta C_1 + i\omega\epsilon l_o C(1 + \frac{1}{3}\omega^2 l_o^2 \epsilon LC)}{1 - \omega^2 \Delta C_1 l_o L(1 + \frac{1}{3}\omega^2 l_o^2 \epsilon LC)} \tag{2-35}$$

where ϵ, l_o, C and L refer respectively to the dielectric constant of the sample, the distance between the two Kel-F plugs, the shunt capacitance and series inductance per unit length of the section line under consideration. The second term in the denominator of (2-35) is found to be $\sim 5 \times 10^{-3}$ at 225 MHz and will be neglected.

For the next transformation that is to give us Y_t, we need to know where Y_t starts and this is determined by the length of the reference lead B_2 (cf. fig. 2-3). This can only be determined experimentally, but by proper choice of B_2, the length of this third section may be made small, leading to (cf. eq. (2-22))

$$Y_t = \frac{Y_2 + i\omega\Delta C_3}{1 + i\omega\Delta L_3 Y_2} \qquad (2\text{-}36)$$

Measuring the empty cell allows us to evaluate $\Delta C_1 + \Delta C_3$, and this is found to be about one half pF. Therefore, the denominator of (2-36) is also approximated to be 1 leading to the simplification

$$Y_t = i\omega(\Delta C_1 + \Delta C_3) + i\omega\epsilon l_o C(1 + \frac{1}{3}\omega^2 l_o^2 \epsilon LC) \qquad (2\text{-}37)$$

Since L and C are known, and $\Delta C_1 + \Delta C_3$ and l_o are accessable to experimental determination, this formula gives us the desired relation between ϵ and Y_t for the liquid filled cell. Specifications for the two different cells used for the experiments are listed in table 2-1.

TABLE 2-1. Cell characteristics.

	$\log_{10}\frac{b}{a}$	$Z_o = \sqrt{\frac{L}{C}}$	C	l_o	$A = \Delta C_1 + \Delta C_3$
cell I	0.6021	83 ohm	40 pF/m	2.17 cm	0.75 pF
cell II	0.4277	59 ohm	56 pF/m	2.61 cm	0.45 pF

In order to obtain a solid sample in the cell at some desired temperature, the material must be introduced as a liquid, frozen slowly, and cooled. During this process gaps and cracks will be formed in the sample due to the difference in thermal expansion coefficients of dielectrics and metals, and resulting strains at the interface of sample and inner conductor. This is not a reversible process and different experiments must be expected to

give different void formations. We now assume that the measurable electric effects of a particular void formation at a temperature T may be analyzed from the model pictured in fig. 2-5, where we

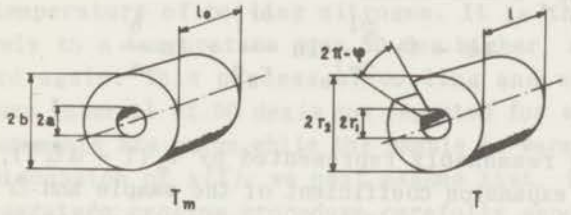

Fig. 2-5. Void formation model. The drawing labelled T_m represents sample just below melting point. The drawing at the right shows sample at some lower temperature T.

have resolved all voids in bulk contractions along cylindrical coordinates. The sample at the melting point T_m fills the whole capacitor, thus having vital dimensions a, b, l_o, and 2π. Then at T_m, ϵ is related to Y_t according to eq. (2-37), which for lower frequencies reduces to

$$Y_t = i\omega(A + B\epsilon) \tag{2-38}$$

with

$$cB = \frac{2\pi l_o}{\ln \frac{b}{a}} \tag{2-39}$$

where c is a unit conversion factor. Now, at some appreciably lower temperature T the sample will have different dimensions, r_1, r_2, l and ϕ, while the conductors, to a good approximation, are still characterized by the quantities a, b, l_o and 2π. In general r_1, r_2, l and ϕ will be functions of T, of the thermal expansion coefficient of the sample, and of the way by which T has been reached. So $r_1 \neq a$ if the sample has been at temperatures lower than T. If we take the dielectric constant of the gas filling the gaps to equal one, we find using standard potential

theory that the observed apparent ϵ_a, linked to Y_t by (2-38) and (2-39), is related to the actual ϵ of the sample material by

$$cB\epsilon_a = \frac{2\pi l_o\{1 + (\epsilon - 1)\frac{\phi l}{2\pi l_o}\}}{(\epsilon - 1)\frac{\phi l}{2\pi l_o}\ln\frac{br_1}{r_2 a} + \ln\frac{b}{a}} \qquad (2\text{-}40)$$

Now l will be reasonably represented by $l_o(1 - \alpha\Delta T)$, where α is the linear expansion coefficient of the sample and $\Delta T = T_m - T$. The temperature dependence of ϕ is expected to show irregularities, but is approximated as $2\pi(1 - \alpha\Delta T)$. Inserting these two expressions gives for the numerator of (2-40)

$$2\pi l_o\{\epsilon - (\epsilon - 1)2\alpha\Delta T\}$$

Neglecting the second term will introduce an error smaller than 5% and allows us to write eq. (2-40) as

$$\epsilon_a = \frac{\epsilon}{(\epsilon - 1)x + 1} \qquad (2\text{-}41)$$

with

$$x \approx (1 - 2\alpha\Delta T)\ln\frac{br_1}{r_2 a} / \ln\frac{b}{a} \qquad (2\text{-}42)$$

The amount of sample present in the cell does not change with temperature; hence the volume of the sample is a function of T only. Therefore, r_1 and r_2 are not independent of each other, and at some temperature the magnitude of either one determines the other. Comparing the two extreme cases $r_1 = a$ and $r_2 = b$ (i.e. a cylindrical gap between the sample and the outer and inner conductor respectively), we find that the resulting effect, expressed by the magnitude of x, is much larger in the latter case. This shows that x is much more dependent on the location of the voids than on their volume. Since we have no means of

predicting the location of cracks, we consider $x(T)$ in eq. (2-41) as an empirical parameter from now on.

At this point it seems appropriate to describe the thermal history of a particular sample by the time it is measured. After the sample in the cell has been solidified, the system is cooled to the temperature of boiling nitrogen. It is then allowed to warm slowly to a temperature some 50 deg higher, after which it is cooled again. This process of cooling and warming over a temperature interval of 50 deg is now repeated for each frequency, and measurements are taken while the sample is warming. Returning to our discussion of $x(T)$, we next assume that, if we go about this temperature cycling procedure carefully enough, $x(T)$ will after the first few cycles be dependent on T only and no longer on the thermal history. Thus it is implied that some fixed location of voids is established. Then $x(T)$ is a regular univalued function of T for the sample under investigation and is the same for measurements at different frequencies (different warming runs). Experimentally the parameter $x(T)$ is derived from low frequency measurements using literature values[7,8] for the static $\epsilon_0(T)$, and the assumptions stated may be checked (cf. chapter 3). The values of x so obtained are of order 0.05. Once $x(T)$ has been determined, the complex dielectric constant $\epsilon = \epsilon' - i\epsilon''$ can be obtained at any frequency and temperature from Y_t by means of eqs. (2-37), (2-38) and (2-41).

We notice that the relation (2-41) between ϵ_a and ϵ, both considered as functions of frequency, is a bilinear transformation in the terminology of the theory of functions. This implies that when the Cole-Cole plot of either one of these quantities is either a semicircle or a circular arc with parameter α (cf. chapter 1), then so is the plot of the other.

2-4. INVESTIGATED COMPOUNDS

In order to provide an unambiguous basis for a theoretical explanation of measured solid state phenomena, it is desirable that experimental data be obtained from single crystal measurements, preferably along the different crystal axes. Unfortunately, at the present state of the art, this is beyond realization for

dielectric measurements on solid hydrogen halides. The data presented refer to polycrystalline samples obtained by slowly freezing the liquid materials.

HYDROGEN IODIDE

Commercially available hydrogen iodide of 98.0% min. stated purity displayed, when collected and molten in a glass container, a red color indicating the presence of iodide. As hydrogen iodide gas at room temperature decomposes easily under influence of light, we performed all distilling in a system with glass parts covered to exclude light. Repeated distillation of the original material in vacuum over anhydrous phosphorous pentoxide resulted in a slightly yellow, almost colorless liquid. The solid, obtained upon freezing, was completely colorless. After these repeated distillations for purification purposes, the cell for dielectric measurements was connected to the system and approximately 5 cc of sample distilled into the cell, where it condensed as a snowy solid somewhere above the upper Kel-F plug (cf. fig. 2-4). Once the desired amount of sample was collected, dry nitrogen gas of one atmosphere pressure was led into the system and the cell allowed to warm in order to melt the sample. The temperature of the cell was then maintained a few deg above the melting point long enough to let the liquid hydrogen iodide fill up the 3 cc sample space in between the two Kel-F spacers. The temperature was then lowered slowly and the liquid frozen from the bottom of the cell. A final decision, whether the sample was acceptable for measurements, was made after the cell was connected to the measuring apparatus and the apparent static dielectric constant (cf. section 2-3) at some temperature could be determined. The magnitude of this static quantity ϵ_a is an indication whether the cell is properly filled (i.e. whether the once liquid hydrogen iodide occupied all available sample space). Comparison of different filling attempts allows us to establish a rough criterium for the quality of a particular sample. Measurements at all frequencies were taken for each "good" sample and data evaluated as discussed in the previous sections from the measured admittances.

HYDROGEN BROMIDE

Hydrogen bromide was purified and handled by the same procedure. The stated purity of the commercially available compound was 99.8% min. Upon liquefaction the liquid obtained was observed to be completely colorless. Small white particles were observed sometimes in the liquid, in agreement with reports by earlier investigators[7,8], and are believed to have been one or more of the hydrogen bromide hydrates. Their presence in the final samples must be assumed.

2-5. TEMPERATURE MEASUREMENT AND CONTROL

Previous investigations on the dielectric relaxation behaviour of hydrogen iodide and hydrogen bromide indicate that for frequencies up to 250 MHz the temperature range of interest lies below 120° K. Use of liquid nitrogen as a refrigerant allows us, by suitable cooling techniques, to lower the temperature of a system to the triple point of nitrogen. The cooling apparatus finally employed for the present investigation was originally developed for a different cell system which was abandoned at a later stage of the experimental work because of unsatisfactory results. It has successively been adapted to later cell designs. As a result, the final version displays some inessential features and is not considered to be the most desirable setup for the kind of experiments undertaken. For instance, temperatures below the nitrogen boiling point could not well be realized.

The cooling system, pictured in fig. 2-6, consisted of two hollow cylindrical concentrical dewar vessels. The inner vessel does not have double walls and is called a dewar vessel for convenience of discussion only.

The outer dewar, made of glass, has a capacity of about 1.5 liter. The space between the double walls can be evacuated or filled with some gas of desired pressure. This dewar rests on a wooden platform and is packed on the outside with one inch thick insulating foam plastic. The level of liquid nitrogen in the dewar may be sensed with the device pictured. This consists of two resistors with appreciable temperature coefficient placed at fixed heights and forming part of a conventional bridge circuit,

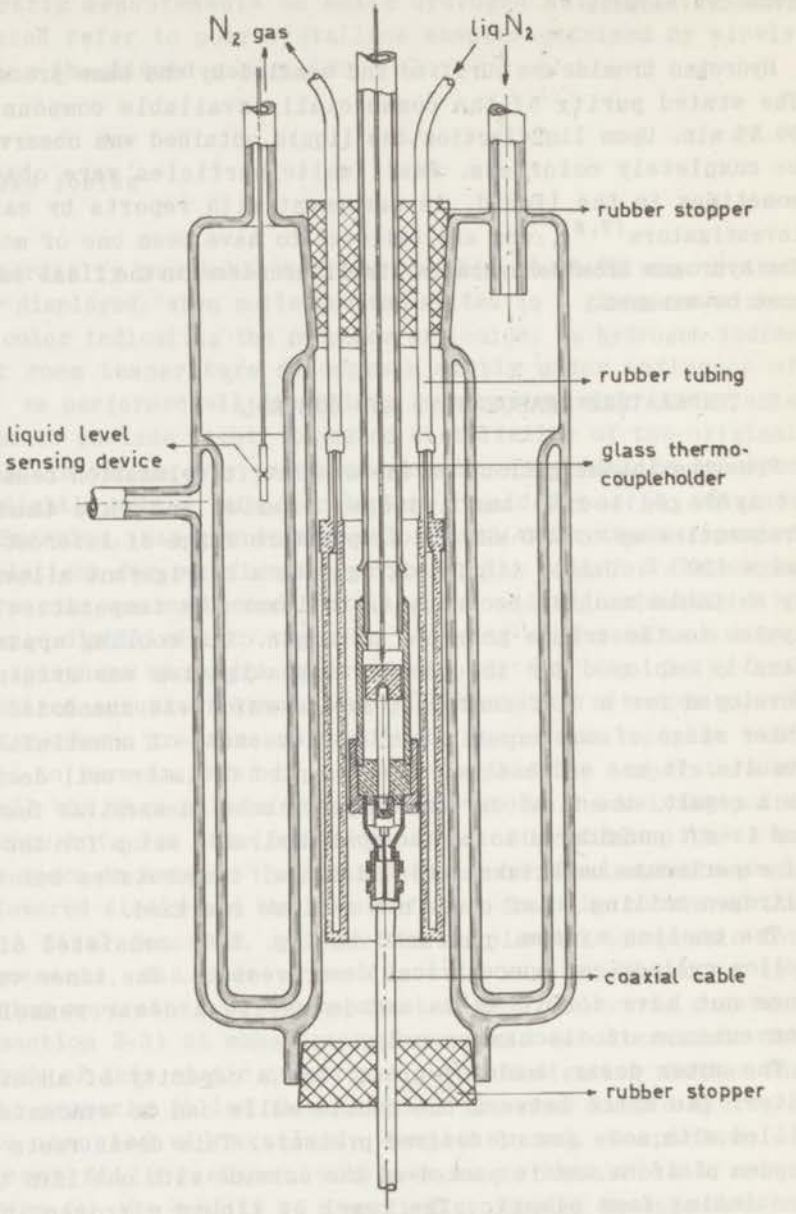

Fig. 2-6. Longitudinal section of the cooling system. Shown concentrically are the glass outer dewar, brass inner cooling vessel, and stainless steel cell.

thus allowing us to read from an ammeter, whether the liquid nitrogen level is below, between, or above the two resistors.

The one pound brass inner dewar, with a capacity of about 40 cc, is suspended by two thin stainless steel rods from the rubber stopper, which closes the top opening of the outer dewar.

The cell occupying the inner space is suspended from a point above the cooling system where also a valve closes the glass tubing shown. Copper wire is wrapped around the cell in order to improve thermal contact with the brass dewar, so that only a small temperature difference can exist between these two metal bodies. The electrical leads from the cell to the admittance meter (via the line system discussed) pass through a rubber stopper which closes the bottom of the system.

The procedure used to control the temperature of the cell containing the sample may be summarized as follows. The outer dewar is kept filled at all times with liquid nitrogen above a certain level, as checked by the indicator. The inner system, i.e. the brass dewar and the cell, is cooled to the boiling point of liquid nitrogen by adding refrigerant to the inner dewar. When we stop this supply, the liquid nitrogen present in the brass dewar will boil away in about 10 minutes, because of heat leakage through the suspension rods of the brass vessel, the electrical (copper) leads through the bottom, and the gas present between the metal system and the rubber stoppers. Next the brass dewar together with the cell will start warming due to the same heat leakage. The rate of warming may be controlled by means of the gas present in the jacket space of the glass outer dewar (helium or nitrogen, of desired pressure). For measurements at different frequencies, taken while the sample is warming, this procedure is to be repeated as many times as there are frequencies of measurement.

Temperatures were measured with a copper-constantan thermocouple in the cell just above the upper Kel-F plug as indicated in the picture. This implies that the measuring metal joint, protected by a glass holder, is surrounded by sample material, but is about one inch away from the midpoint between the two Kel-F spacers. In connection with the rather high warming rates of the samples

while measurements were taken, the question arises, whether the temperatures so measured are representative. Fortunately, it was possible to get some insight in this problem, since hydrogen bromide exhibits a sharp phase transition in the temperature interval studied. This transition temperature has been used to obtain a correction to the measured temperatures (cf. chapter 3). In this connection we may mention that the apparent attractiveness of constant temperature experiments is somewhat questionable in the present case, since measurements on HBr and DBr performed under isothermal conditions have been found[7,8] to show time dependent behaviour of ϵ (the initial values being restored upon appreciable temperature variation). Sufficiently complete frequency coverage in the presently investigated range would require more than five hours. Measurements of thermocouple EMF values were performed with a high resolution potentiometer (Leeds and Northrup Type K-2) and temperatures calculated with the aid of standard temperature vs. EMF tables[9]. The thermocouples used were calibrated at the melting point of ice, the freezing point of mercury, the sublimation point of carbon dioxide and the boiling point of commercial liquid nitrogen. From these, corrections to the standard tables were determined, which amounted to 15 μV at the nitrogen boiling point.

REFERENCES

(1) *Instruction Manual for the* RX-*Meter type* 250-A, (Boonton Radio Company, Rockaway, N.J., U.S.A.).
(2) S.E. Lovell, Ph.D. thesis, Brown University, (1958).
(3) P.J.M. v. Heteren, dissertatie, R.U. Leiden, (1966).
(4) R.H. Cole, unpublished notes.
(5) N.L. Brown and R.H. Cole, J. Chem. Phys. **21**, 1920 (1953).
(6) R.W. Swenson and R.H. Cole, J. Chem. Phys. **22**, 284 (1954).
(7) S.H. Havriliak, Jr., Ph.D. thesis, Brown University, (1958).
(8) N.L. Brown, Ph.D. thesis, Brown University, (1952).
(9) H. Schenker, J.I. Lauritzen, R.J. Corrucini and S.T. Lonberger, *Reference Tables for Thermocouples*, Natl. Bur. Std. (U.S.) Circ. No. 514 (1951).

CHAPTER 3

EXPERIMENTAL RESULTS

3-1. HYDROGEN IODIDE

Results are presented of series of measurements on two different samples of hydrogen iodide, each sample series consisting of eight different frequency runs. By a frequency run we name the set of admittance measurements taken at constant frequency for different temperatures in the region studied. In the following we refer to the two series as the 3rd and 4th series (other ones were discarded because of reasons stated in chapter 2, page 52). The cells labelled I and II, whose characteristics have been described in section 2-3, were used for the 3rd and 4th series respectively.

A typical output of admittance measurements for hydrogen iodide is shown in fig. 3-1, where the original coordinates, $\Delta Y_x/i\omega$ vs. thermocouple EMF, have been rescaled to show ϵ_a (hence not corrected for line loss and cell inductance) and T. Approximately one sixth of all points measured in the temperature region considered are shown.

The effects of the various corrections discussed in detail in the second chapter are illustrated in table 3-1. In columns the admittances at the successive stages of the data evaluation are given with the appropriate corrections applied. The three highest frequencies only are shown, as for the lower ones most corrections are negligible (except for the void correction). It is seen from this table (step 2) that the correction due to the residual inductance L_s in series with the C_4 capacitor in the bridge circuit may amount to as much as 17% at 225 MHz. The determination of the value of L_s, accurate to 10%, has been performed with the aid of purely capacitative components. It is questionable, however, how well the proposed simple scheme represents the circuit characteristics at higher frequencies, especially when components

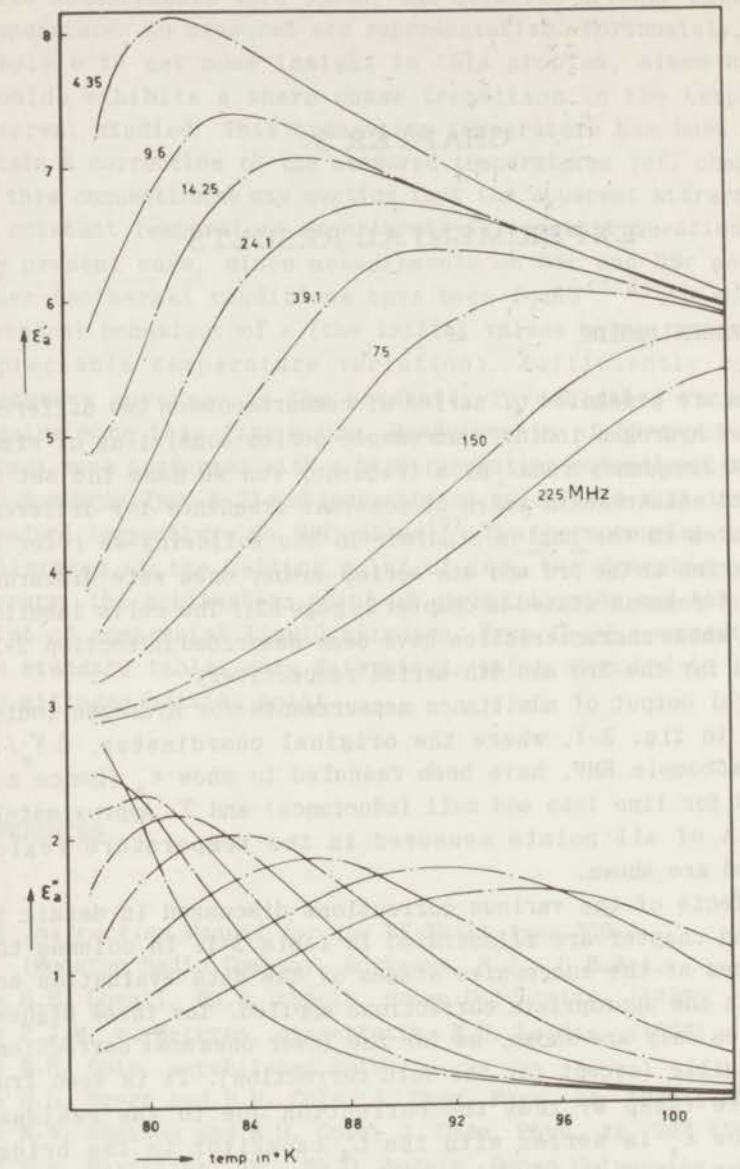

Fig. 3-1. Temperature dependence of ϵ_a at various frequencies, HI, 4th sample series.

with appreciable conductance are measured. Similarly, errors introduced by possible improper tuning of the coupling lines (cf. chapter 2, page 43) will be felt most seriously at the higher frequencies. From these considerations, it is estimated that the probable error in ϵ_a is 5% for the two highest frequencies and 3% or better for the other ones.

TABLE 3-1. Successive corrections applied to measured admittances; HI, 4th series, -5.444 mV (80 K).

	75 MHz	150 MHz	225 MHz
$\Delta\ Y_p/i\omega \times 10^{12}$	5.41	4.64	4.15
	-1.80 i	-1.25 i	-0.91 i
1 dial calibration			
$\Delta\ Y_4/i\omega \times 10^{12}$	5.44	4.64	4.15
	-1.80 i	-1.25 i	-0.91 i
2 bridge residuals			
$Y_x/i\omega \times 10^{12}$	5.53	4.96	4.85
	-1.80 i	-1.25 i	-0.91 i
3 line loss			
$Y_t/i\omega \times 10^{12}$	5.53	4.97	4.86
	-1.79 i	-1.24 i	-0.88 i
4			
$(Y_t - i\omega A)/i\omega l_o C$	3.41	3.03	2.96
	-1.22 i	-0.84 i	-0.60 i
5 cell inductance			
ϵ_a	3.40	3.01	2.92
	-1.22 i	-0.83 i	-0.58 i
6 voids in sample			
ϵ	3.88	3.39	3.29
	-1.80 i	-1.15 i	-0.79 i

More serious errors are introduced in step 6, mainly because of the following difficulty. Thermocouple EMF recordings were taken while the sample was warming at a rate of approximately 1 deg

every two minutes the actual rate depending on temperature and on the thermal conditions of a particular warming run. A possible temperature difference between the thermocouple cold junction and the sample would result in systematic errors in the temperature indications. Hence similar thermocouple EMF recordings for different warming runs may correspond to different temperatures. This may be illustrated by the following kind of analysis. The void correction applied in step 6 has been shown to be reasonably represented by

$$\epsilon_a = \frac{\epsilon}{(\epsilon-1)x + 1}, \quad \text{or} \quad \frac{1}{\epsilon_a} = \frac{1}{\epsilon} + (1-\frac{1}{\epsilon})x \qquad (3\text{-}1)$$

At some fixed frequency and temperature, ϵ will be a constant and ϵ_a will be a function of x, which we consider for the moment as a running parameter. The transformation is pictured in fig. 3-2 and $\epsilon_a(x)$ is found to lie on a circle through the points 0, 1, and ϵ.

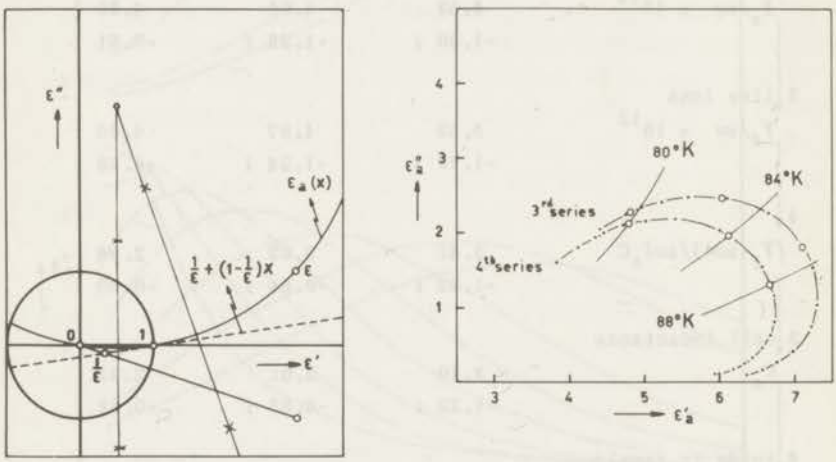

Fig. 3-2. Graphical representation of the transformation $\epsilon_a = \frac{\epsilon}{1 + (\epsilon-1)x}$ with x as running parameter.

Fig. 3-3. Constant frequency complex plane loci for ϵ_a, 3rd and 4th series HI, 24.1 MHz. Open points correspond to same thermocouple EMF readings.

Applying this graphical method to the constant temperature ϵ_a loci at the same frequency, obtained from two different sample series, we are able to draw the $\epsilon_a(x)$ circles for individual temperatures, as has been done in fig. 3-3. The ϵ_a values corresponding to the same temperature should lie on the same circle. As can be seen, appreciable discrepancies are found, indicative of the seriousness of the aforementioned difficulty. The same ambiguity may hold for temperature indications of the different frequency runs of one sample series. Elimination of this problem is not well possible without affecting the significance of the results. Therefore we used the same table (calibrated as discussed in chapter 2) to convert thermocouple EMF values into °K for both measurement series and all frequency runs. Hence constant temperature data are obtained from fig. 3-1 by drawing vertical lines corresponding to desired temperatures and reading the ordinates of the intersections with the constant frequency ϵ_a curves. One rough check on the obtained temperatures is possible as HI displays a phase transition near 125°K. From the present measurements we obtain for the phase transition temperature 125.5 ± 0.5°K. This is to be compared with the literature values 125°K[1], 126°K[2], ~125°K[3].

Another difficulty can be noticed by inspection of fig. 3-1. At higher temperatures the lower frequency data should show negligible dispersion, in particular the $\epsilon'_a(T)$ curves for 4.35 MHz and 9.6 MHz should coincide at temperatures higher than 100°K. Since they do not, we have to conclude that the location of voids has been different for these two frequency runs. This conclusion is supported by the fact that the 4.35 MHz measurements headed the row of the eight frequencies in measuring sequence. For this reason, the ϵ_a values of the 4.35 MHz run of the 4th series were corrected such that the corrected values coincided with the higher frequency ϵ_a values at higher temperatures (eq. (3-1) with $x = -0.004$). Similar but larger discrepancies were found in the 3rd series. For this series we preferred not to apply a correction of this kind, but to discard runs that showed appreciable high temperature deviations.

Still another source of error associated with step 6 is the necessity of using literature data to evaluate the correction parameter x, with the result that any errors in these earlier data are introduced automatically into the present ones.

In view of the fact that errors in the present ϵ data are

introduced mainly with the application of the void correction, we want to investigate what conclusions may be drawn from the obtained ϵ_a numbers to which this correction has not yet been applied. Fig. 3-4 shows complex plane loci for ϵ_a. From previous

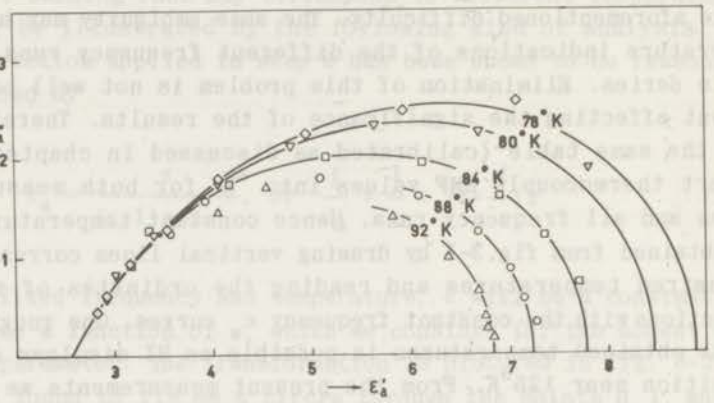

Fig. 3-4. Constant temperature complex plane loci for ϵ_a, HI, 4th series. Frequencies from right to left: 4.35, 9.6, 14.2[5], 24.1, 39.1, 75, 150, 225 MHz.

investigations[2,4] we know that the low frequency dielectric behaviour of hydrogen iodide is of the Debije type, i.e. the low frequency parts of the Cole-Cole plots for ϵ are circles that intersect the real axis perpendicularly. Because of the bilinear transformation connecting ϵ and ϵ_a the same must hold for the ϵ_a loci. For this reason semicircles have been drawn in fig. 3-4 to fit the lower frequency points. It is seen that the loci have skewed arc appearance (cf. chapter 1 for nomenclature and formulae of the different shapes of Cole-Cole plots). It is concluded that the ϵ_a loci are neither a semicircle, nor a circular arc, nor a linear superposition of more of these shapes with well separated relaxation times. Because of the bilinear transformation connecting ϵ and ϵ_a the same conclusions hold without ambiguity for the Cole-Cole plots of ϵ.

Information of more quantitative character can be obtained from the high frequency behaviour of ϵ_a. The ϵ_a loci warrant the conclusion that the high frequency behaviour is properly described

by a skewed or circular arc formula. For $\omega\tau \gg 1$ both these formulae may be written as

$$\frac{\epsilon'_a - \epsilon_{a\sim}}{\epsilon''_a} = \operatorname{cotg}\phi, \qquad \text{with } \phi \frac{2}{\pi} = \beta,\ 1 - \alpha \tag{3-2}$$

Assuming $\epsilon_{a\sim}$ and ϕ to be temperature independent (justifiable over a small temperature range), we can determine these parameters from constant frequency data. Least squares analysis has been applied to the 225 MHz measurements at temperatures between 78°K and 83°K with the results given in table 3-2. The angle parameter remains

TABLE 3-2. Least squares determination of parameters $\epsilon_{a\sim}$ and β in the equation $\epsilon'_a = \epsilon_{a\sim} + \epsilon''_a \cdot \operatorname{cotg} \frac{\pi}{2} \beta$ applied to n different temperature ϵ_a data of the 225 MHz results, HI.

measuring series	n	$\epsilon_{a\sim}$	$\epsilon_\sim$	β
3rd	5	2.71	3.10	0.68
4th	8	2.60	3.06	0.66

the same upon transformation of ϵ_a to ϵ and has direct significance for the Cole-Cole plots. We want to stress the importance of this result as this analysis uses temperature as a running parameter and hence eliminates the temperature difficulties mentioned earlier. Upon inspecting higher order terms in the $1/\omega\tau$ series expansion (3-2) we find that the obtained β values should be considered as lower limits, the actual values being a few percent larger. The shown $\epsilon_\sim$ values are calculated from the $\epsilon_{a\sim}$ values using the void correction as will be discussed below.

Finally, the parameter x necessary for the application of the void correction was evaluated by the following procedure. The circles drawn in fig. 3-4 and justified by the literature information[2,4] on the low frequency behaviour of ϵ_{HI} at temperatures higher than 70°K allow fairly accurate determination of the zero frequency values of ϵ_a for temperatures higher than

80°K. These $\epsilon_{ao}(T)$ values combined with literature data[2,4] on $\epsilon_o(T)$ allow us to calculate $x(T)$ with the aid of eq. (3-1). The parameter $x(T)$ was found to be almost temperature independent, and for each measurement series we used one value of x for all temperatures considered. Once the value of x is evaluated, all $\epsilon_a(\omega,T)$ numbers are transformed into $\epsilon(\omega,T)$ values with the aid of eq. (3-1). The graphical representation of the transformation has been discussed in connection with fig. 3-2. The magnitude of the correction is demonstrated in table 3-3. The general effect of the correction is to enlarge and displace the ϵ_a locus, its shape remaining approximately unaltered, while the individual

TABLE 3-3. Void correction applied to ϵ_a data for hydrogen iodide.

	3rd series, 80°K $x = 0.046$		4th series, 88°K $x = 0.058$	
freq. in MHz	ϵ_a	ϵ	ϵ_a	ϵ
4.36	8.24	12.49	7.21	11.65
	-1.95 i	- 4.95 i	-0.33 i	- 0.92 i
9.6	7.34	10.12	7.13	11.44
	-2.76 i	- 6.24 i	-0.57 i	- 1.57 i
14.25			7.01	11.09
			-0.82 i	- 2.21 i
24.1	4.79	5.58	6.68	10.14
	-2.25 i	- 3.60 i	-1.24 i	- 3.15 i
39.1	3.96	4.47	6.08	8.66
	-1.65 i	- 2.37 i	-1.60 i	- 3.68 i
75	3.45	3.85	5.09	6.53
	-1.01 i	- 1.37 i	-1.79 i	- 3.47 i
150	3.07	3.38	3.93	4.61
	-0.74 i	- 0.96 i	1.57 i	- 2.51 i
225	2.97	3.26	3.57	4.13
	-0.59 i	- 0.76 i	-1.24 i	- 1.87 i

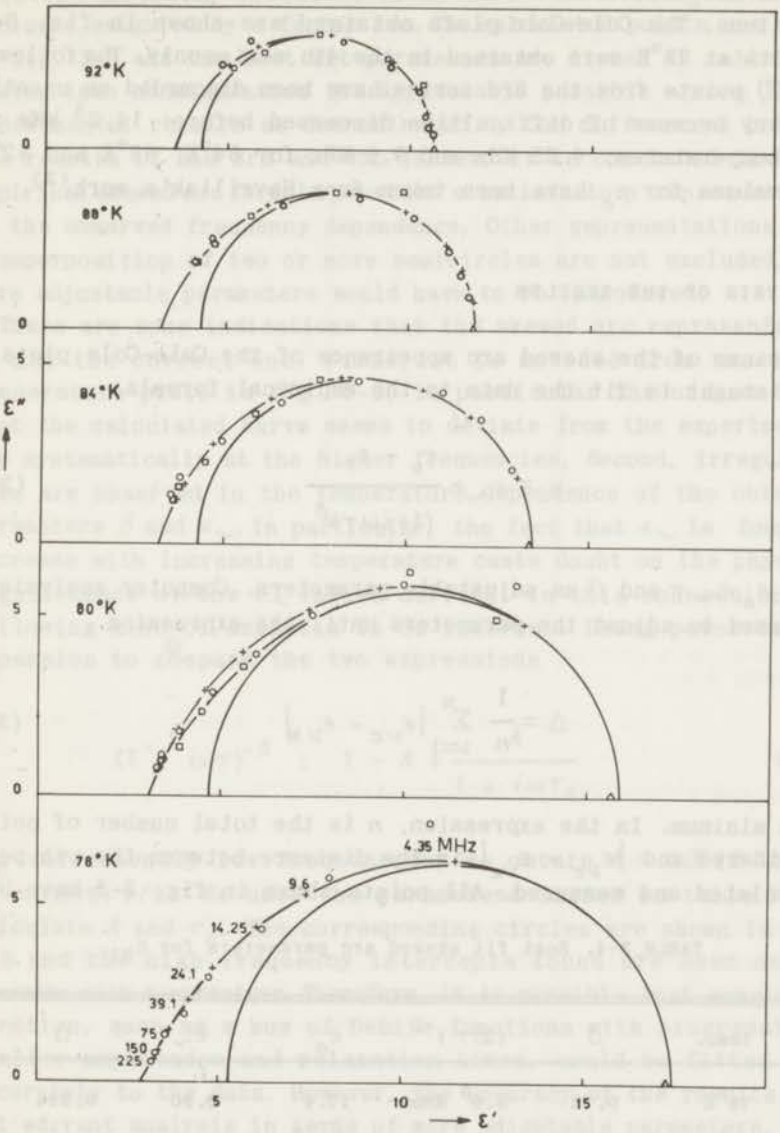

Fig. 3-5. Cole Cole plots for ϵ_{HI}.
○ 4th series, + calculated skewed arc points
□ 3rd series, △ static ϵ_o data (Havriliak).

points are shifted over the curve to apparently higher frequency positions. The Cole-Cole plots obtained are shown in fig. 3-5. Results at 78°K were obtained in the 4th series only. The following $\epsilon(\omega,T)$ points from the 3rd series have been discarded as unsatisfactory because of difficulties discussed before: 14.2^5 MHz for all temperatures; 4.35 MHz and 9.6 MHz for 84°K, 88°K and 92°K. The values for ϵ_o have been taken from Havriliak's work[2].

ANALYSIS OF THE RESULTS

Because of the skewed arc appearance of the Cole-Cole plots we have sought to fit the data to the empirical formula

$$\epsilon = \epsilon_\sim + \frac{\epsilon_o - \epsilon_\sim}{(1+i\omega\tau)^\beta} \tag{3-3}$$

with $\epsilon_o, \epsilon_\sim, \tau$ and β as adjustable parameters. Computer analysis[5] was used to adjust the parameters until the expression

$$\Delta = \frac{1}{n} \sum_{\nu=1}^{n} |\epsilon_{\nu c} - \epsilon_{\nu m}| \tag{3-4}$$

is a minimum. In the expression, n is the total number of points considered and $|\epsilon_{\nu c} - \epsilon_{\nu m}|$ is the distance between the νth point calculated and measured. All points shown in fig. 3-5 have been

TABLE 3-4. Best fit skewed arc parameters for ϵ_{HI}.

temp.	β	$(2\pi\tau)^{-1}$	ϵ_o	$\epsilon_\sim$	Δ
78°K	0.72	3.6^5 MHz	17.4	2.90	0.314
80°K	0.78	6.9 MHz	15.9^5	3.05	0.395
84°K	0.82	18.4 MHz	13.4	3.25	0.306
88°K	0.77	35.8 MHz	11.8	3.22	0.220
92°K	0.82	73.5 MHz	10.6^5	3.58	0.161

used for analysis, while the literature values of ϵ_o have been included weighted by a factor two. The calculated points are shown in fig. 3-5 and the best fit parameters are listed in table 3-4. Taking into consideration the appreciable possible errors in the experimental results as demonstrated by the differences between the results of the 3rd and 4th series, it is concluded that the empirical skewed arc formula provides a satisfactory representation of the observed frequency dependence. Other representations like a superposition of two or more semicircles are not excluded, but more adjustable parameters would have to be introduced.

There are some indications that the skewed arc representation is not the correct one. First, it is noticed from the lower temperature plots in fig. 3-5, in particular the one at 80°K, that the calculated curve seems to deviate from the experimental one systematically at the higher frequencies. Second, irregularities are observed in the temperature dependence of the obtained parameters β and $\epsilon_\sim$. In particular, the fact that $\epsilon_\sim$ is found to increase with increasing temperature casts doubt on the physical significance of the $\epsilon_\sim$ values derived. In this connection the following kind of analysis is of interest. Using power series expansion to compare the two expressions

$$(1 + i\omega\tau)^{-\beta} \quad ; \quad 1 - A + \frac{A}{1 + i\omega\tau_d} \tag{3-5}$$

for sufficiently low frequencies, we obtain $A = 2\beta/(\beta+1)$ and $\tau_d = (\beta+1)\,\tau/2$. We used the parameters listed in table 3-4 to calculate A and τ_d. The corresponding circles are shown in fig. 3-5 and the high frequency intercepts found are seen not to increase with temperature. Therefore, it is possible that some other function, such as a sum of Debije functions with progressively smaller amplitudes and relaxation times, could be fitted more accurately to the data. However, the accuracy of the results does not warrant analysis in terms of more adjustable parameters.

The temperature dependence of the relaxation times derived is investigated in the usual way. The rate plot is shown in fig. 3-6 and the equation

$$\log_{10}\tau = \frac{662}{T} - 15.9 \tag{3-6}$$

represents the observed temperature dependence within experimental error.

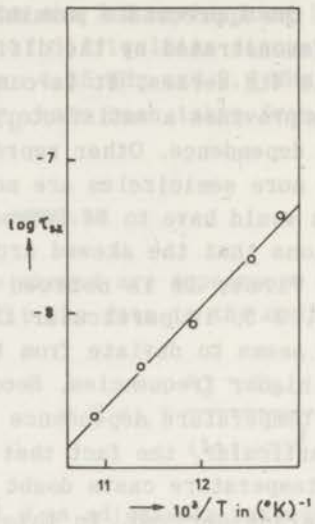

Fig. 3-6. Rate plot for skewed arc relaxation times, HI, as listed in table 3-4.

COMPARISON WITH PREVIOUS INVESTIGATIONS

The frequency dependence of the dielectric constant of hydrogen iodide at temperatures between 70°K and 80°K has been investigated by Havriliak [2,4] in the frequency range of 15 Hz to 500 kHz. His results could be interpreted on basis of Debije behaviour and the temperature dependence of the relaxation time was fitted by the equation

$$\log_{10}\tau = \frac{778}{T} - 17.23 \qquad (3\text{-}7)$$

The present results at 88°K and 92°K confirm that the frequency dependence for sufficiently low frequencies can be described in terms of one single relaxation time. As anticipated by Havriliak,

this description fails for higher frequencies, whereas the skewed arc formula is found to be a good approximation. To compare the relaxation times we have to use the quantities τ_d from equation (3-5) representative for low frequency Debije behaviour. Fig. 3-7

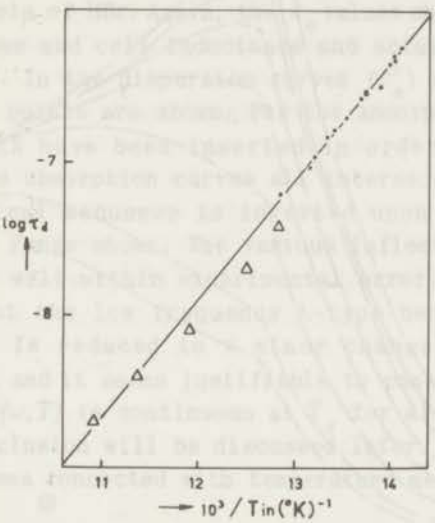

Fig. 3-7. Rate plot for Debije relaxation times, HI.
. Havriliak[2,4]
Δ present investigation: τ_d calculated with formula (3-5)

shows the totality of results. The straight line is the one determined by eq. (3-7). The deviations of the lower temperature points obtained in the present investigation are thought to be due to failure of the comparison approach (3-5) rather than experimental errors. For, at these temperatures (78°K, 80°K), parameters are compared, which have been obtained from measurements at frequencies for which $\omega\tau \ll 1$ and $\omega\tau > 1$ respectively.

3-2. HYDROGEN BROMIDE

Experimental results obtained in series of admittance measurements on two different samples of hydrogen bromide, hereafter called the 1st and 4th series, are presented. Both samples were

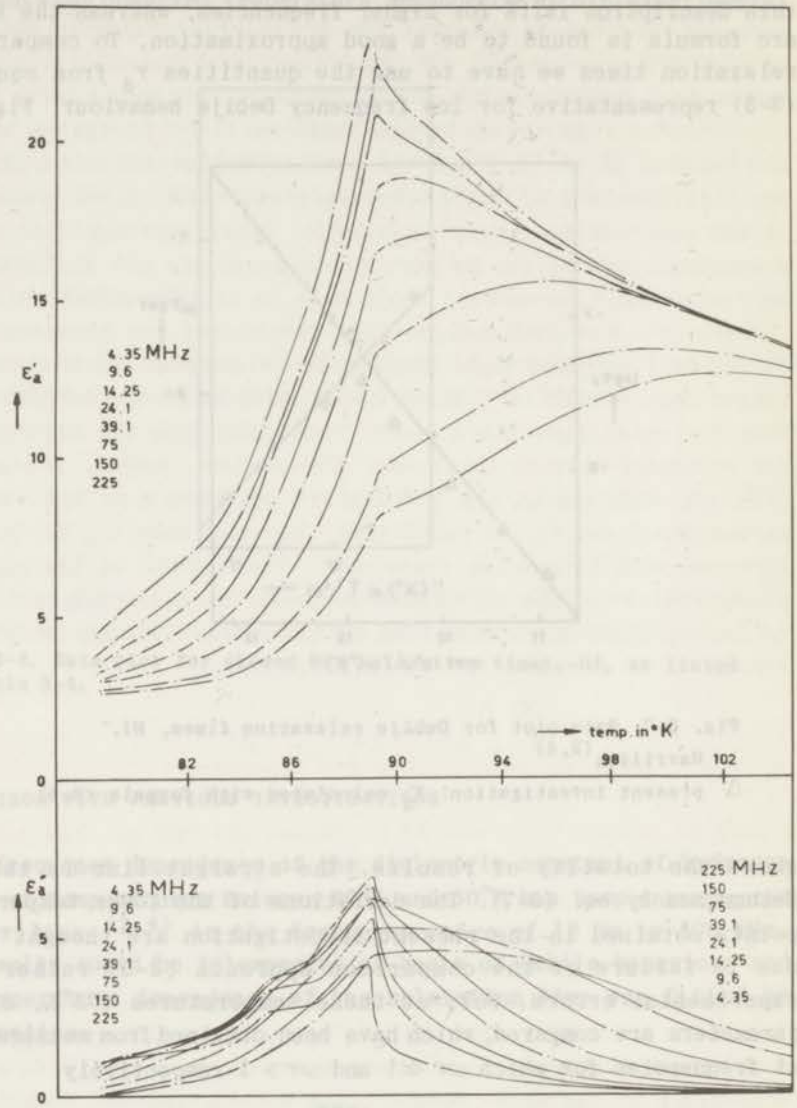

Fig. 3-8. Temperature dependence of ϵ_a at various frequencies, HBr, 1st sample series.

measured in cell I. The temperature range in which relaxation behaviour could be investigated extends from 80°K to 100°K. At ~ 89°K, HBr displays a λ-type solid phase transition, observable by a sharp peak in the low frequency dielectric constant.

Fig. 3-8 shows measured admittances obtained with a slowly warming sample of HBr. Again, the ϵ_a values shown are not corrected for line loss and cell inductance and actually represent $(\Delta Y_x - i\omega A)/i\omega l_o C$. In the dispersion curves (ϵ'_a) about half the number of measured points are shown. For the absorption curves (ϵ''_a) only a few points have been inserted in order not to obscure the picture. The absorption curves all intersect each other once and their vertical sequence is inverted upon passage through the temperature range shown. The various inflection points have been established well within experimental error. It is seen from the figure, that the low frequency λ-type behaviour of ϵ'_a at the transition is reduced to a minor change in slope at higher frequencies, and it seems justifiable to conclude from the present data that $\epsilon(\omega,T)$ is continuous at T_c for all ω. The implications of this conclusion will be discussed later.

The problems connected with temperature measurements made under

TABLE 3-5. Solid phase transition temperatures hydrogen bromide.

investigation	observable	transition temperatures in °K		
present	ϵ			
1st series (warming)		89.5 ± 0.2*	112.7 ± 1.2	115.5 ± 1.2
4th series (warming)		88.4 ± 0.2	112.2 ± 1.0	115.0 ± 1.0
Brown[7,8]	ϵ			
sample 11-1 (cooling)		88.7	112.0	117.0
sample 19-1 (cooling)		89.1	112.7	117.0
sample 19-1 (warming)		-	114.2	117.3
Giauque, Wiebe[6]	C_v	89.5	113.4	116.9

* The indicated precision is related to the inaccuracy of the graphical evaluation of the transition temperatures. The absolute errors in the given temperatures are larger.

nonisothermal conditions have been discussed amply in the previous section. Table 3-5 shows that the lowest transition temperature, observed with two different samples, varies by 1°K. The values of the three solid phase transition temperatures, measured in the 1st series are in satisfactory agreement with ones obtained from heat capacity measurements[6]. Evaluation of ϵ data from the obtained admittance measurements involves use of static $\epsilon_o(T)$ data measured by Brown[7,8]. Therefore our temperatures were corrected to agree with the λ-transition temperature obtained by Brown (T_c = 89.1°K). The T_c correction obtained (different for the two series) was added as a constant to the measured temperatures above T_c, while below T_c the correction was interpolated linearly to be zero at 80°K. In fig. 3-9 the graphical analysis of constant frequency ϵ_a diagrams developed in the previous section is shown.

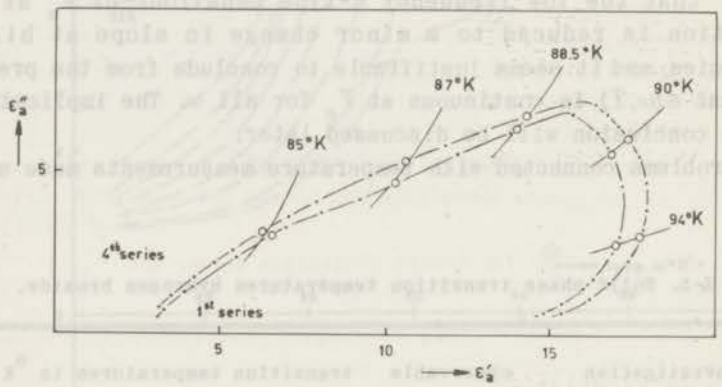

Fig. 3-9. Constant frequency complex plane loci for ϵ_a, HBr, 1st and 4th series, at 39.1 MHz. Open points refer to corrected temperatures.

The consistency of the obtained temperature scales is confirmed for temperatures higher than 87°K. This check is not a completely independent one as it is assumed that both samples consisted of the pure compound. Discrepancies for lower temperatures cannot be eliminated. Temperatures measured during different frequency runs in one sample series are fairly consistent as may be seen from fig. 3-8.

Distinct changes in relaxation behaviour occur upon passage through the λ-transition and accordingly results on the two different solid phases are reported separately.

HIGHER TEMPERATURE PHASE, $T > 89°K$

The calculation of ϵ data from the measured admittances follows the procedure developed in chapter 2. The corrections for line loss and cell inductance are somewhat larger than for the HI measurements as the measured admittances are larger. Complex plane loci for ϵ_a are given in fig. 3-10. The low frequency Debije behaviour

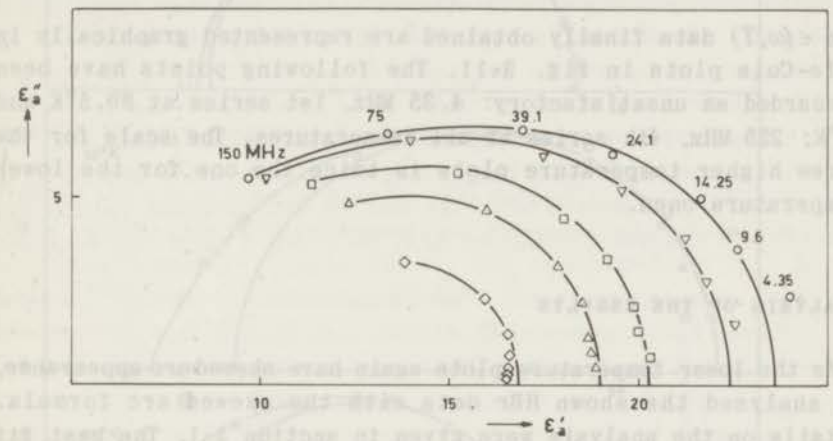

Fig. 3-10. Constant temperature complex plane loci for ϵ_a, HBr, 4th series, higher temperature phase. Temperatures from largest to smallest curve: 89.5, 90, 92, 94, 98°K.

observed in earlier investigations[7] is conclusively confirmed by the present results. A high frequency analysis, as applied in section 3-1, is not possible in the present case, as now the condition $(\omega\tau)^{-1} \ll 1$ is not sufficiently satisfied (cf. eq. (3-2)). The semicircles in fig. 3-10 fitting the lower frequency data were used to find static $\epsilon_{ao}(T)$ values. The void correction parameter x was evaluated with the aid of literature $\epsilon_o(T)$ values[7]. For HBr, the temperature dependence of $x(T)$ could not be neglected as it could for HI. Since no anomalies in the thermal expansion coefficient of HBr have been reported[9,10] we fitted the observed temperature dependence of $x(T)$ to a linear one, justifiable by series expansion of $x(T_c - T)$ in the small temperature range considered. The values of x obtained are shown in table 3-6.

TABLE 3-6. Void correction parameters for HBr measurements, higher temperature phase.

	$x(T)$
1st series	$0.0324 - 0.0006(T-T_c)$
4th series	$0.0306 - 0.0007^5(T-T_c)$

The $\epsilon(\omega,T)$ data finally obtained are represented graphically in Cole-Cole plots in fig. 3-11. The following points have been discarded as unsatisfactory: 4.35 MHz, 1st series at 89.5°K and 90°K; 225 MHz, 4th series at all temperatures. The scale for the three higher temperature plots is twice the one for the lower temperature ones.

ANALYSIS OF THE RESULTS

As the lower temperature plots again have skewed arc appearance, we analysed the shown HBr data with the skewed arc formula. Details on the analysis were given in section 3-1. The best fit parameters are listed in table 3-7 and the points corresponding

TABLE 3-7. Best fit skewed arc parameters for ϵ_{HBr}, higher temperature phase.

temp. in °K	β	$(2\pi\tau)^{-1}$	ϵ_o	ϵ_∞	Δ
89.5	0.63	7.71 MHz	88.7	4.19	2.052
90	0.64	12.9 MHz	69.7	4.63	1.185
92	0.75	34.6 MHz	47.2	7.36	0.968
94	1.09	79.5 MHz	37.2	11.60	0.563
98	2.72	316 MHz	26.9	16.7	0.362

to the frequencies of measurement calculated with these parameters are shown in fig. 3-11. It is seen that the empirical formula represents the measured frequency dependence within experimental error, possibly with exception of the highest frequency points.

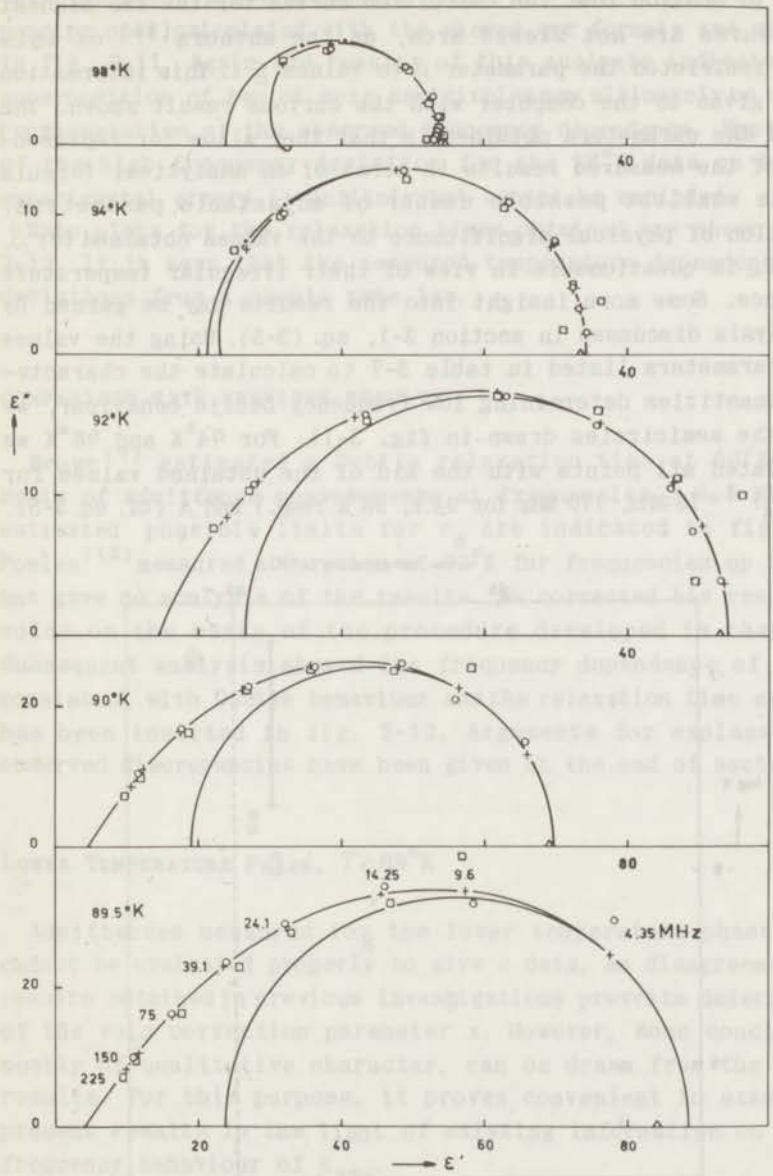

Fig. 3-11. Cole Cole plots for ϵ_{HBr}, higher temperature phase,
○ 4th series, □ 1st series, $\Delta\epsilon_o$(Brown[7,8])
\+ calculated with skewed arc formula
. calculated with Debije formula

We want to mention that the calculated curves for the two highest temperatures are not skewed arcs, as the authors[11] of this formula restricted the parameter β to values ≤ 1. This information was not given to the computer with the curious result shown. The merit of the parameters obtained is that they allow for representation of the measured results in terms of an analytical formula with the smallest possible number of adjustable parameters. Attribution of physical significance to the values obtained for β, τ, and ϵ_∞ is questionable in view of their irregular temperature dependence. Some more insight into the results may be gained by the analysis discussed in section 3-1, eq. (3-5). Using the values of the parameters listed in table 3-7 to calculate the characteristic quantities determining low frequency Debije behaviour, we obtain the semicircles drawn in fig. 3-11. For 94°K and 98°K we recalculated all points with the aid of the obtained values for $\tau_d((2\pi\tau_d)^{-1}=76$ MHz, 170 MHz for 94°K, 98°K resp.) and A (cf. eq. 3-5).

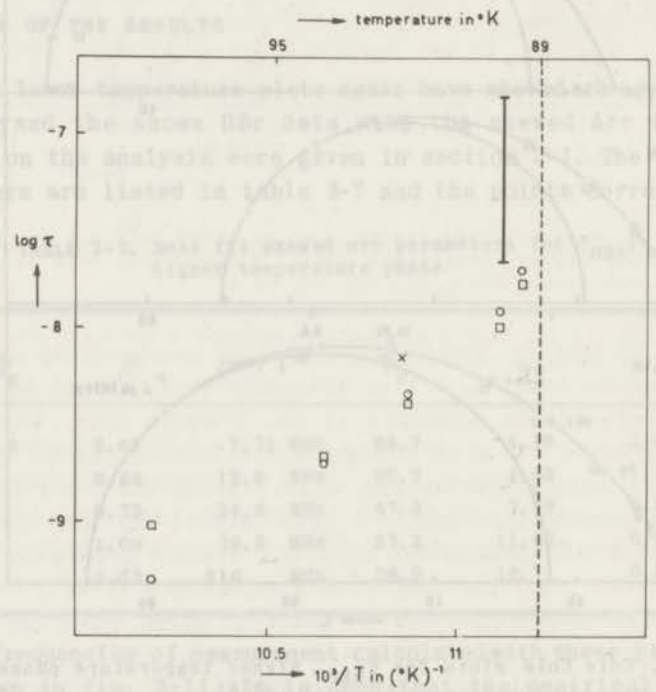

Fig. 3-12. Rate plot for relaxation times HBr.
○ τ_{sa} (table 3-7), □ $\tau_d = (\beta+1)\,\tau_{sa}/2$, × Powles[12], I Brown[7]

Only the two highest frequency points are different from corresponding ones calculated with the skewed arc formula and are shown in fig. 3-11. Again the results of this analysis indicate that a superposition of two or more semicircles may ultimately be a better representation of the observed frequency dependence. Explanation of the high frequency deviation for the 98°K data on basis of experimental errors is unlikely but cannot be excluded.

Rate plots for the relaxation times obtained are shown in fig. 3-12. It is seen that the measured temperature dependence shows deviations from a simple rate law.

COMPARISON WITH PREVIOUS RESULTS

Brown[7] estimated a Debije relaxation time at 90°K on the basis of admittance measurements at frequencies $\leqq 0.5$ MHz. The estimated possible limits for τ_d are indicated in fig. 3-12. Powles[12] measured absorption at 92°K for frequencies up to 7 MHz but gave no analysis of the results. We corrected his results for voids on the basis of the procedure developed in chapter 2. Subsequent analysis showed the frequency dependence of ϵ to be consistent with Debije behaviour and the relaxation time evaluated has been inserted in fig. 3-12. Arguments for explanation of observed discrepancies have been given at the end of section 3-1.

LOWER TEMPERATURE PHASE, $T < 89°K$

Admittances measured for the lower temperature phase of HBr cannot be evaluated properly to give ϵ data, as disagreement with results obtained in previous investigations prevents determination of the void correction parameter x. However, some conclusions, mostly of qualitative character, can be drawn from the present results. For this purpose, it proves convenient to examine the present results in the light of existing information on the low frequency behaviour of ϵ_{HBr}.

Typical constant temperature complex plane loci for ϵ_a are shown in fig. 3-13. It is seen that the high frequency behaviour has features similar to those found in the higher temperature phase, the angle of skew incidence being slightly smaller now.

This appearance will remain unchanged when the shown data are corrected for voids with the aid of the formula discussed before.

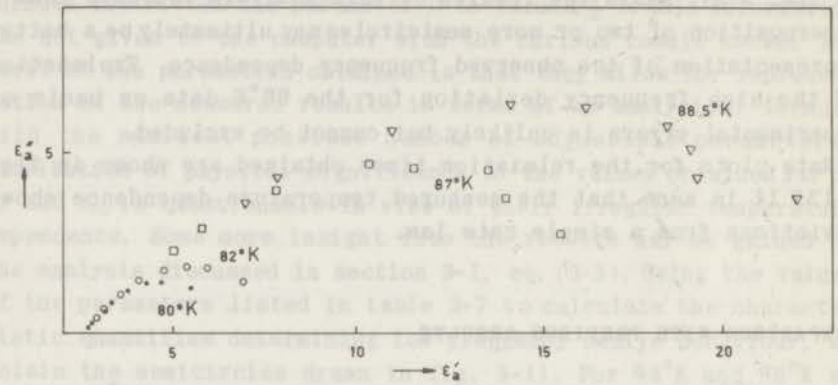

Fig. 3-13. Constant temperature complex plane loci for ϵ_a, HBr, 1st series, lower temperature phase. Frequencies from right to left: 4.35, 9.6, 14.2^5, 24.1, 39.1, 75, 150, 225 MHz.

Earlier investigations[7,12] have revealed that HBr in the lower temperature phase displays two dispersion regions with associated characteristic times of order 10^{-3} and 10^{-6} respectively. In the following we refer explicitly to results obtained by Brown[7,8] at frequencies below 5 MHz. These results were found to be consistent with a lineair superposition of two circular arcs, the high frequency one having $\alpha = 0$ at temperatures higher than 80°K. His data for the low frequency circular arc were used to calculate its contribution to $\epsilon(\omega,T)$ at 4.35 MHz and 87.5°K to be 0.5 and 1 for ϵ' and ϵ'' respectively. The contributions to ϵ'_a and ϵ''_a are smaller. At 82°K these contributions are ~ 0.1. Hence we conclude that the existence of the low frequency dispersion and absorption does not noticeably manifest itself at frequencies $\geq$ 4.35 MHz and temperatures $\leq$ 87.5°K.

From the foregoing it is clear that, in order to determine the correction parameter x, zero frequency extrapolations of the present results should be compared with high frequency limits ϵ_1 obtained by Brown for the low frequency circular arc (measured in the kHz region). Values of $x(T)$ determined this way were found to be unacceptable. For instance, present results give for ϵ_{ao} (87°K) a value > 15, while Brown lists a value of 13.6 at 87.5°K for the corresponding quantity ϵ_1, leading to a negative value of x. As no anomalies for the thermal expansion coefficient at T_c

have been reported[9,10] we have no reason to expect $x(87°K)$ to be very different from its value 0.03 at T_c. Errors in the presently reported temperatures are possible, certainly in view of the large heat capacity of HBr near T_c, but not to the extent that they could provide an explanation for the discrepancy mentioned. An attempt for explanation will be given later.

Conclusions drawn from $\epsilon_a(\omega, T)$ behaviour have qualitative significance for ϵ, as the consequences of the void correction are mainly of quantitative character with little effect on the form of dependence on ω and T.

The present results for 80°K and 82°K (cf. fig. 3-13) show that the high frequency dispersion cannot be represented by a circular arc with $\alpha = 0$. Combination of these present results with Brown's data at 81.5°K for frequencies from 1 to 5 MHz strongly suggest that the complete picture in the high frequency range again forms a skewed arc or at least has a very similar appearance. Using $x(T_c)$ to correct ϵ_a data at 80°K and 82°K for voids and analysing for skewed arc parameters, we obtain $\epsilon_\infty \sim 2.5$, $\beta \sim 0.6$, $\tau_{sa} = 5.4$ MHz at 80°K and 5.7 MHz at 82°K. The derived zero frequency values ϵ_1 (7.5 and 9.7 resp.) are larger than values obtained by Brown ($\epsilon_1 = 7$ at 81.5°K).

From figs. 3-8 and 3-9 it is seen that $\epsilon_a(\omega, T)$ is continuous at T_c. Ignoring for convenience of discussion the existence of the low frequency dispersion in the kHz region, we formally represent the present low temperature phase data by the same analytical formula (skewed arc) used at $T > T_c$, as suggested by the results at 80°K and 82°K. The observed continuity of $\epsilon_a(\omega, T)$ at T_c then implies that all parameters, considered as functions of T, have to be continuous at T_c. In this connection it is interesting to examine the temperature dependence of f_m, the frequency of maximum absorption (maximum ϵ''). From fig. 3-13 it is seen that f_{am}, the frequency for which ϵ''_a is a maximum, increases from 10 MHz at 80°K to 40 MHz at 88.5°K fitting smoothly to the value 50 MHz at 89.5°K in the higher temperature phase (fig. 3-10). This value for f_{am} of 50 MHz at 89.5°K was found after correcting for voids with $x = 0.03$ to correspond to $f_m \sim (2\pi\tau_d)^{-1} \sim 10$ MHz. If we correct the lower temperature phase data of ϵ_a for voids with $x = 0.03$, the values of f_m obtained are almost temperature independent and equal to ~ 10 MHz. In spite of the uncertainty with respect to precise numerical values of the results, we believe that the

deduced behaviour of f_m is in principle correct and significant. Values for f_m obtained after correcting the ϵ_a data with $x(T_c)$ are plotted in fig. 3-14 as indicated.

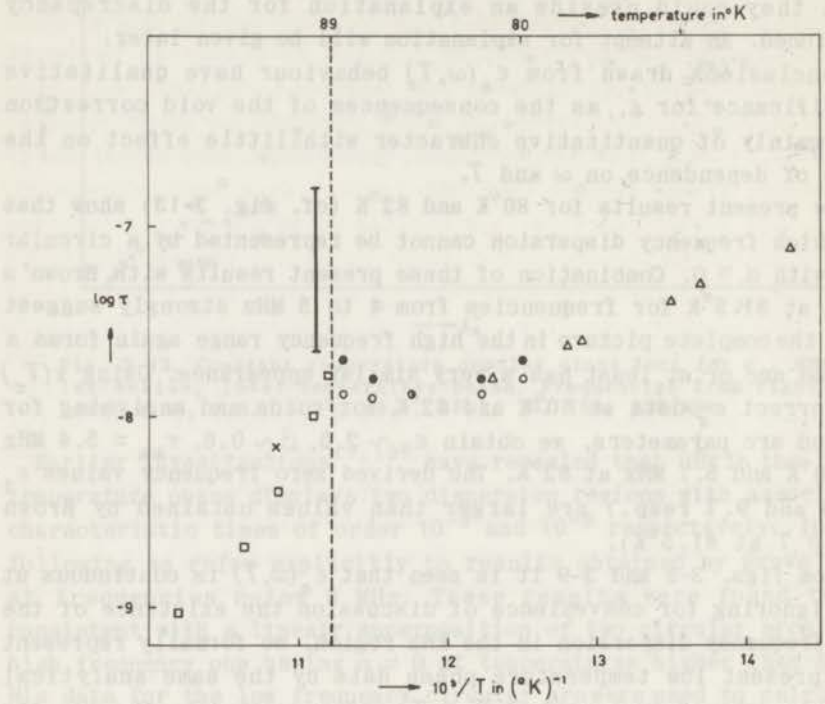

Fig. 3-14. Rate plot for HBr relaxation times, associated with frequencies of maximum absorption: $(2\pi\tau_m)^{-1} = f_m$

□ $\tau_d = (\beta+1)\tau_{sa}/2$, I,Δ Brown[7], × Powles[12]

○,● $\tau_m = (2\pi f_m)^{-1}$, 1st and 4th series resp.

COMPARISON WITH PREVIOUS RESULTS

As mentioned before, discrepancies with Brown's earlier data are found. Representing the dielectric behaviour of HBr at temperatures below $T_c = 89°K$ by

$$\epsilon = \epsilon_\infty + (\epsilon_1 - \epsilon_\infty)F_1(i\omega\tau_1) + (\epsilon_o - \epsilon_1)F_2(i\omega\tau_2) \qquad (3\text{-}8)$$

as suggested by earlier investigators, the differences between present and previous results may be summarized as follows:

1. Values for ϵ_1 consistent with results obtained in the present investigation increase faster with temperature between 80°K and 89°K than found previously, while the obtained value for $\epsilon_1(80°K)$ agrees reasonably with Brown's value.

2. $F_1(i\omega\tau_1)$ at 80 and 82°K is presently found to be of skewed arc type with $\beta \sim 0.6$, rather than a circular arc with $\alpha = 0$ (Brown) or $\alpha \neq 0$ (Powles), proposed on basis of measurements at frequencies lower than 5 MHz.

It is seen from fig. 3-14 that the presently obtained characteristic times are in satisfactory agreement with literature values, as far as comparison is possible.

3-3. DISCUSSION

The empirical void correction parameter x, necessary for calculation of dielectric constants from the measurements, has been determined by comparing present results with ones obtained by earlier investigators. An unambiguous calculation of x is not possible, but the consistency of the values obtained may be demonstrated with the aid of the void formation model proposed in chapter 2, page 49. The correction formula $\epsilon_a = \epsilon / \{(\epsilon - 1)x + 1\}$ accounts for any arrangement of cylindrical voids, and its application introduces errors smaller than 5% if x can be determined accurately. In first approximation (cf. chapter 2)

$$x \approx \ln \frac{br_1}{r_2 a} / \ln \frac{b}{a} \approx f\left(\frac{b}{a}\right) \alpha \Delta T / \ln \frac{b}{a} \qquad (3\text{-}9)$$

where b and a are conductor radii, r_1 and r_2 are sample radii, α is the linear expansion coefficient of the sample material, $\Delta T = T_m(\text{melting point}) - T$, and f is a factor $1 \leqq f \leqq \frac{b}{a}$ dependent on the radial location of the voids. Values for α determined from X-ray measurements[3], or estimated with Grüneisen's rule have been used for calculation of the results shown in table 3-8. Deduced values of f do not differ by more than 10% from their arithmetic mean.

TABLE 3-8. Comparison of calculated and observed values of x for different cells and different sample materials at 90°K.

	HI 3rd series	HI 4th series	HBr 1st series	HBr 4th series
cell	I	II	I	I
$\log \frac{b}{a}$	0.602	0.428	0.602	0.602
$\alpha \Delta T$	0.022	0.022	0.017	0.017
$(2.3\ x/f)_{calc}$	0.037	0.052	0.029	0.029
x_{obs}	0.046	0.058	0.032	0.031

In view of this consistency it is estimated that errors in the x values determined do not exceed 10%. The presupposition that the earlier ϵ_o data used for calculation are correct is implied in this estimate. Errors due to this and other causes render the final ϵ data about 10% uncertain, while somewhat larger errors must be reckoned with for the HBr data at temperatures below and just above T_c. On this basis the proposed empirical dispersion formula was decided to be representative for the results observed, and listing of associated best fit parameters chosen for presentation of the obtained experimental evidence. The present data do not completely justify the analytical form of the skewed arc function or attribution of physical significance to the parameters. The values obtained for the static dielectric constant ϵ_o agree closely with literature data because of the calculation procedure applied. The skewed arc relaxation times τ certainly are characteristic times as long as the concept characteristic is not explicitly specified. However, other quantities introduced like τ_d, representing low frequency Debije behaviour, or $\tau_m = (2\pi f_m)^{-1}$ where f_m is the frequency of maximum loss ϵ''_m, all have the same dimension and order of magnitude. The quantity $\epsilon_\sim$ results from extrapolation of high frequency data, and presumably corresponds to a limiting value for ϵ at $\omega\tau = O(10^6)$ only if the formula used for extrapolation accounts for the complete dielectric behaviour. In this case $\epsilon_\sim$ should coincide with the long wave

limit of the square of the refractive index $n_\sim^2$. An estimate for $n_\sim^2$ is obtained with the aid of the Lorentz-Lorenz relation

$$\frac{n_\sim^2 - 1}{n_\sim^2 + 2} = \frac{4\pi}{3} N_o \alpha_o \frac{\rho}{M} \qquad (3\text{-}10)$$

where N_o is Avogadro's number, α_o is the polarizability of an individual molecule, ρ is the density, and M the molecular weight of the material under consideration. With the aid of values for α_o determined from gas phase dielectric experiments[13], and X-ray data for ρ[3,14], the quantity $n_\sim^2$ may be calculated with results shown in table 3-9. The temperature dependence of $n_\sim^2$ between

TABLE 3-9. Comparison of the quantities $n_\sim^2$ and $\epsilon_\sim$ for hydrogen halides.

	HI	HBr
α_o	5.5×10^{-24} cm^3 (13)	3.5×10^{-24} cm^3 (13)
M	128 g	81 g
ρ	3.57 g cm^{-3} at 77°K (3)	2.85 g cm^{-3} at 90°K (14)
$n_\sim^2$	2.9 at 77°K	2.4 at 90°K
$\epsilon_\sim$	2.9 at 80°K 3.6 at 92°K	2.5 at 80°K 4.6 at 90°K

80°K and 100°K is negligible (variation <2%). It is seen that the agreement between $n_\sim^2$(calc.) and $\epsilon_\sim$(obs.) is surprisingly good at 80°K, a temperature at which the available frequencies are sufficiently high to allow fairly accurate extrapolation. Discrepancies at higher temperatures demonstrate that the empirical function with best fit parameters does not represent the complete dielectric behaviour. Hence values of $\epsilon_\sim$ obtained for temperatures higher than 80°K do not have immediate physical significance. As the best fit analysis closely relates resulting values for $\epsilon_\sim$ and β, especially when relatively low frequency data are used, physical significance, if any, of the parameter β can only be attributed to the lower temperature data. The value $\beta \sim$ 0.68 (table 3-2) obtained from constant frequency data analysis

for HI at temperatures between 78°K and 83°K seems to be the most reliable value for this parameter found in this investigation. In fact, constant temperature complex plane diagrams of the normalized function $(\epsilon - \epsilon_\infty)/(\epsilon_0 - \epsilon_\infty)$ for HI with $\epsilon_\infty = 2.9$ and for the higher temperature phase of HBr with $\epsilon_\infty = 3.5$ closely fit a skewed arc curve with $\beta = 2/3$ at all temperatures. However, significant deviations from the required frequency distribution are found.

Data for the low temperature phase of HBr show clearly that the high frequency behaviour is similar to that found at temperatures above T_c. The evidence for the temperature independence of f_m between 80°K and $T_c = 89$°K, and the rapid increase of ϵ_1 (cf. eq. (3-8)) in the same temperature interval is not altogether conclusive. Important in this connection seems to be the evidence reported by earlier investigators[2,4,7,8] that samples of HBr and DBr are not stable under isothermal conditions at temperatures below T_c. At constant temperature considerable changes (up to 25%) were observed in $\epsilon(\omega)$ as function of time, the frequency dependence remaining qualitatively unaltered. We believe that the present data do not show indications for such behaviour. We may mention, however, that the crystal structures of the investigated compounds are anisotropic, and that the polycrystalline samples of the different investigations were subjected to quite different thermal cycles and constraints. As a result, the measured average properties could well be different because of different distributions (possibly time dependent) of variously oriented regions (cf. remark at the end of section 1-2). A satisfactory explanation of this macroscopic effect will require a systematic investigation. This demonstrates, however, that the quantitative significance of values for the constants ϵ_0 and ϵ_1 obtained in various investigations is subject to some doubt. As associated changes in characteristic frequencies were found to be small (DBr)[2] or zero (HBr)[7], we believe that the presently found $f_m(T)$ behaviour (cf. fig. 3-14) must be qualitatively correct.

Closely related is the question of continuity of $\epsilon(\omega,T)$ at T_c. The evidence provided by the present investigation cannot be claimed to be altogether conclusive for two reasons. The frequencies employed are too high to detect the kHz region dispersion and hence provide no information about the temperature dependence of the low frequency dispersion "amplitude" $\Delta_1\epsilon = \epsilon_0 - \epsilon_1$, cf. eq. (3-8). Thermal inhomogeneity of the samples used may obscure

a possible discontinuity in the $\epsilon(\omega, T_c)$ data. We feel, however, that in particular the smooth character of the constant frequency complex plane plots (cf. fig. 3-9) strongly suggests that $\epsilon(\omega, T)$ is continuous at T_c. Implications are that the λ-behaviour must be ascribed to $\Delta_2\epsilon = \epsilon_1 - \epsilon_\infty$, while $\Delta_1\epsilon$ falls of to zero as the transition temperature is approached.

Clearly the changes in dielectric relaxation behaviour at the λ-transition are not the same for both hydrogen halides studied. Above T_c, both HI and HBr show skewed arc type dispersion and absorption at more or less comparable frequencies. This relaxation "mode" is continued below T_c but its character changes to circular arc type behaviour, as this shape has been conclusively established by earlier investigators at temperatures several degrees below T_c. In addition HBr displays below T_c another circular arc mode at much lower frequencies. Interpretation of these observations can best be made in terms of the electric moment correlation function $\bar{\Phi}(t)$ introduced in chapter 1. For the present discussion $\bar{\Phi}(t)$ (normalized) and $\epsilon(\omega)$ are considered scalar functions. $\bar{\Phi}(t)$ is obtained from $\epsilon(\omega)$ by inverse transform of the relation[15]

$$\frac{\epsilon - \epsilon_\infty}{\epsilon_o - \epsilon_\infty} = \{1 + E\,[\{\mathcal{L}(-\dot{\bar{\Phi}})\}^{-1} - 1]\}^{-1} \qquad (3\text{-}11)$$

where E is a (scalar) local field factor and $\mathcal{L}(\ )$ indicates the Laplace transform is to be taken. For skewed arc type dispersion, found in the higher temperature phase, the result is

$$\bar{\Phi}_{sa}(t) = E \sum_{n=1}^{\infty} \frac{(1-E)^{n-1}}{\Gamma(n\beta)} \Gamma(n\beta, t/\tau_{sa}) \qquad (3\text{-}12)$$

where $\Gamma(n,x)$ is the incomplete gamma function. The circular arc correlation function corresponding to the same relaxation mode below T_c is

$$\bar{\Phi}_{ca}(t) = \sum_{n=o}^{\infty} \frac{\{-E(t/\tau_{ca})^{1-\alpha}\}^n}{\Gamma\{n(1-\alpha)+1\}} \qquad (3\text{-}13)$$

while for HBr the complete behaviour is described by a linear combination of two such functions (corresponding to F_1 and F_2 in eq. (3-8)). The short time behaviour of the two correlation functions (3-12) and (3-13) is given by

$$\tilde{\Phi}_{sa}(t) = 1 - E\frac{(t/\tau_{sa})^{\beta}}{\Gamma(\beta+1)} + \ldots \qquad (3\text{-}14)$$

$$t/\tau \ll 1$$

$$\tilde{\Phi}_{ca}(t) = 1 - E\frac{(t/\tau_{ca})^{1-\alpha}}{\Gamma(2-\alpha)} + \ldots \qquad (3\text{-}15)$$

which expressions are similar if the corresponding parameters are comparable. Values for β of order 2/3 presently found compare favourably with values for α of order 1/3 determined earlier[2,7] at sufficiently low temperatures, while the respective characteristic times may be called roughly consistent although their temperature dependence cannot be represented by one simple rate law as shown by fig. 3-14 (the behaviour of f_m at the HI λ-transition has similar features[2,4]). Therefore the important conclusion may be drawn that the short time behaviour of $\tilde{\Phi}$ is unaffected by the changes in dynamic behaviour associated with the phase transition. The existence of the additional mode for HBr is irrelevant for this conclusion as it is characterized by much longer times. For comparison of long time behaviour asymptotic expansions of the functions (3-12) and (3-13) are needed. These may be obtained by integration[16] of known expansions[17,18] for the functions $-\dot{\tilde{\Phi}}(t)$ resulting in the first terms

$$\tilde{\Phi}_{sa}(t) \sim \frac{E}{(E-1)^2}\frac{\beta}{\Gamma(1-\beta)}\, e^{-t/\tau_{sa}}\,(t/\tau_{sa})^{-\beta-1}\,, \quad E \neq 1 \qquad (3\text{-}16)$$

$$t/\tau \gg 1$$

$$\tilde{\Phi}_{ca}(t) \sim \frac{1}{E\Gamma(\alpha)}\,(t/\tau_{ca})^{-1+\alpha} \qquad (3\text{-}17)$$

It is seen that the circular arc correlation function needs much longer times for decay towards a negligible fraction of $\tilde{\Phi}(0)$. Therefore the changes that occur on traversing the phase transition from the lower to the higher temperature phase may be interpreted in terms of a loss of long time correlation. The disappearance of the additional mode for HBr may be considered even more pronounced evidence of such an effect. The interpretation is valid irrespective of the precise analytical form of the empirical functions involved as the whole argument may be repeated in terms of continuous or discrete distribution functions of relaxation times.

Assuming that the concept of diffusion plays some part in the dynamics governing dielectric relaxation one is tempted to think of some connection between long time behaviour and long range order. The evidence discussed above could then be interpreted as an indication that the phase transition considered involves the disappearance of long range order while the short range order remains essentially unaffected. (The temperature dependence of the static dielectric constant provides similar information, as the expression $\partial S/\partial E^2 \sim \partial \epsilon_o/\partial T$[19], where S and E stand for entropy and electric field, changes sign at T_c.)

A rather heuristic explanation may be given for the anomalous temperature dependence of f_m observed for HBr near T_c. The local field factor E occurring in eq. (3-11) can be considered as a measure for the ratio of macroscopic and microscopic characteristic times. For instance, in the Debije treatment[20] of simple exponential decay the ratio between the macroscopic relaxation time experimentally observed and a microscopic characteristic time having proper physical meaning equals $E = (\epsilon_o + 2)/(\epsilon_\infty + 2)$. In terms of this theory high values of E near a λ-transition would enlarge a macroscopic characteristic time considerably in agreement with the deviations observed. Other treatments[21,22,23,15] restrict the factor E to values $\leqq 3/2$, however the continuum approach involved cannot be expected justifiable for periodic structures in solids.

Another explanation for deviations of a relation $\tau \sim \exp(-\Delta F/RT)$ from usual behaviour might be sought in appreciable temperature dependence near an order disorder phase transition of the entropy term involved.

COMPARISON WITH THEORY

Adam[24] has advanced a molecular kinetic theory of cooperative relaxation processes based on the assumption that loss of orientational correlation is determined by the number of vacancies present in the nearest neighbour coordination shell of a representative molecule. For a random distribution of vacancies, expressions are derived describing dielectric relaxation in terms of a discrete spectrum with as many terms as there are nearest neighbour sites. The quantitative predictions for the higher temperature phase of HBr are not verified by the present experimental results. Qualitatively the results may be said not to contradict Adam's theory as applied to more liquid-like structures characterized by smaller ratios of successive relaxation times. Definite conclusions cannot be drawn as the theory includes several adjustable parameters, while errors in the experimental results render a detailed analysis impossible.

Glarum[25] suggested that the low temperature circular arc behaviour of the hydrogen halides might be explained on basis of a defect diffusion model. The chain reversal mechanism proposed has features of macroscopic domain wall motion and is not likely to represent actual microscopic behaviour. His model in its more general form, however, includes the possibility of a continuous transition from circular arc to skewed arc type behaviour. In view of the presently obtained experimental evidence this property of the model is thought to be very interesting. Unfortunately a proper molecular interpretation of the parameters involved has not yet been made, the treatment being basically a phenomenological one.

Zwanzig[26] studied the effect of rotational Brownian motion on the dielectric susceptibility of a rigid cubic lattice of permanent point dipoles. By means of a high temperature perturbation expansion he showed that dipolar interaction gives rise to a discrete spectrum. At sufficiently low temperatures departure from ideal Debije relaxation should be expected at high frequencies. This result is qualitatively confirmed by the present experimental evidence. Comparison of quantitative character cannot be made as the high temperature expansion of the theory restricts the static dielectric constant to relatively small values.

REFERENCES

(1) W.F. Giauque and R. Wiebe, J. Am.Chem. Soc. **51**, 1441 (1929).
(2) S. Havriliak, Jr., Ph.D. thesis, Brown University, (1958).
(3) F.A. Maurer, C.J. Keffer, R.B. Reeves and D.W. Robinson, J. Chem. Phys. **43**, 1465 (1965).
(4) R.H. Cole and S. Havriliak, Jr., Discussions Faraday Soc. **23**, 31 (1957).
(5) Computer program written by Drs. A.M. Ras, Gaubius Instituut, Leiden.
(6) W.F. Giauque and R.Wiebe, J. Am. Chem. Soc. **50**, 2193 (1928).
(7) N.L. Brown, Ph.D. thesis, Brown University, (1952).
(8) N.L. Brown and R.H. Cole, J. Chem. Phys. **21**, 1920 (1953).
(9) B. Ruheman and F. Simon, Z. Physik. Chem. **15B**, 389 (1931).
(10) G. Natta, Gazz. Chim. Ital. **63**, 425 (1933).
(11) W. Davidson and R.H. Cole, J. Chem. Phys. **19**, 1484 (1951).
(12) J.G. Powles, J. Phys. Radium **13**, 121 (1952).
(13) C.T. Zahn, Phys. Rev. **24**, 400 (1924).
(14) G. Natta, Nature **127**, 235 (1931).
(15) R.H. Cole, J. Chem. Phys. **42**, 637 (1965).
(16) E.T. Whittaker and G.N. Watson, *A course of Modern Analysis*, (Cambridge University Press, New York, 1962) p. 153.
(17) K.S. Cole and R.H. Cole, J. Chem. Phys. **10**, 98 (1942).
(18) B. Gross, J. Applied Phys. **18**, 212 (1947).
(19) C.J.F. Böttcher, *Theory of Electric Polarization*, (Elsevier Publishing Company, Amsterdam, 1952) p. 118.
(20) P. Debije, *Polar Molecules*, (Dover Publications, Inc., New York) p. 90.
(21) L. Onsager, J. Am. Chem. Soc. **58**, 1486 (1936).
(22) J.G. Kirkwood, J. Chem. Phys. **7**, 911 (1939).
(23) S.H. Glarum, J. Chem. Phys. **33**, 1371 (1960).
(24) G. Adam, J. Chem. Phys. **43**, 662 (1965).
(25) S.H. Glarum, Ph.D. thesis, Brown University, (1959).
(26) R. Zwanzig, J. Chem. Phys. **38**, 2766 (1963).

SAMENVATTING

In dit proefschrift worden de resultaten gegeven van enige experimentele en theoretische onderzoekingen naar het diëlectrisch gedrag van de waterstofhalogeniden HI en HBr in hun vaste fasen.

Het eerste hoofdstuk bevat enige inleidende beschouwingen over de theorie van de diëlectrische relaxatie, gevolgd door een overzicht van beschikbare experimentele gegevens betreffende vast HI en HBr. Vervolgens wordt een eenvoudig model voor faseovergangen in vaste waterstofhalogeniden behandeld op basis van klassieke (evenwichts-)statistische mechanica. Het blijkt, dat in een vlakgecentreerd orthorhombisch rooster van permanente puntdipolen een antiferroelectrische faseovergang optreedt. De diëlectrische eigenschappen van het model, toegepast op HBr, worden besproken.

Het tweede hoofdstuk is gewijd aan een discussie van de apparatuur, waarmede de diëlectrische eigenschappen van HI en HBr experimenteel zijn bepaald. Bijzondere aandacht wordt besteed aan problemen, die verband houden met het onvermijdelijk gebruik van electrische verbindingsstukken tussen het meetinstrument en de cel, welke het te onderzoeken diëlectricum bevat. De invloed, die de door verschillen in uitzettingscoefficienten van meetmonster en celwand veroorzaakte inhomogeniteit van de celvulling heeft op de kwantitatieve betekenis van de meetgegevens, wordt onderzocht.

Experimentele resultaten van dispersie- en verliesmetingen aan vast HI en HBr worden gegeven in het derde hoofdstuk. Met de beschikbare frequenties kon het fenomenologische relaxatiegedrag van de onderzochte stoffen bepaald worden in het temperatuurgebied van 80°K tot 100°K. De nadruk is gelegd op grafische presentatie van de gevonden resultaten. De waargenomen frequentieafhankelijkheid van de diëlectrische constante van beide stoffen in hun hogere-temperatuur-fasen kan, binnen de meetnauwkeurigheid, beschreven worden met een enkele empirische scheve-boog-formule. In de discussie wordt de nauwkeurigheid van de meetgegevens besproken en een overzicht gegeven van de verkregen informatie. Mogelijkheden van interpretatie worden aangegeven. Het blijkt dat het relaxatiegedrag in de onderzochte fasen overeenkomst vertoont met het

gedrag van een aantal polaire vloeistoffen. De conclusie, dat de bij de faseovergang van het λ-type optredende veranderingen in het coöperatief moleculair-dynamische gedrag in verband gebracht mogen worden met een wijziging in orde-over-lange-afstand, wordt aannemelijk gemaakt. Enige theorien, voorgesteld ter verklaring van het diëlectrische relaxatiegedrag van waterstofhalogeniden ofwel van vaste stoffen in het algemeen, worden getoetst aan de hand van de verkregen experimentele informatie.

Overeenkomstig de verlangens van de Faculteit der Wiskunde en Natuurwetenschappen volgt hier een overzicht van mijn academische studie.

Het eindexamen voor de opleiding Gymnasium β, gevolgd aan het St. Bernardinuscollege te Heerlen, werd afgelegd in 1957. In het zelfde jaar werd een aanvang gemaakt met de academische studie aan de Faculteit der Wiskunde en Natuurwetenschappen van de Rijksuniversiteit te Leiden. Het candidaatsexamen scheikunde, letter F, werd afgelegd in 1960. Gedurende de daaropvolgende doctoraalstudie ben ik werkzaam geweest op de afdeling Fysische Chemie II van het Laboratorium voor Anorganische en Fysische Chemie te Leiden. Het doctoraalexamen, met als hoofdrichting fysische chemie en als bijvakken toegepaste wiskunde en statistische mechanica, werd afgelegd in 1963 bij de hoogleraren Dr. C.J.F. Böttcher, Dr. C. Visser en Dr. S.R. de Groot. Gedurende de jaren 1964 en 1965 werden de experimentele onderzoekingen, welke aan dit proefschrift ten grondslag liggen, verricht in het Chemistry Department van Brown University, Providence, R.I., U.S.A., onder leiding van Dr. R.H. Cole. De voltooiing van het onderzoek vond plaats in het Gaubius Instituut te Leiden.

I am greatly indebted to Dr. R.H. Cole for his continuous interest in the experimental work and for many instructive discussions during my stay at his laboratory and thereafter. The stimulating discussions I had with Dr. S.K. Kim and Mr. R.S. Wilson and all those who contributed to make my stay at Brown a memorizable one were very much appreciated. Acknowledgement is due to Messrs. R. Holburn, R. Brandon and J. Hall for their aid with the construction of the experimental apparatus. The experimental work was supported by the Advanced Research Projects Agency.

Een woord van dank komt toe aan mijn collegae in Leiden voor hun bijdragen aan het tot stand komen van dit proefschrift. In het bijzonder dank ik mej. Drs. A.M. Ras voor haar welkome hulp bij de computer-analyse van de meetgegevens. Mijn vader ben ik zeer veel dank verschuldigd voor de zorgvuldigheid, waarmee hij de figuren heeft getekend. De vaardige wijze, waarop mej. E. v. Noordt heeft bijgedragen tot het drukklaar maken van het manuscript heb ik bijzonder gewaardeerd. De heer W.J. Brokaar ben ik erkentelijk voor het fotograferen van de tekeningen.

Bijlage academisch proefschrift
P.P.M. Groenewegen, Leiden 1966.

STELLINGEN

1. Indien Kirkwood's theorie betreffende met gehinderde rotatie samenhangende faseovergangen wordt toegepast op een rooster van puntdipolen, worden vrijwel gelijke resultaten verkregen, ongeacht of één dan wel beide termen van de dipool-dipool-interactiepotentiaal in rekening gebracht worden.

Hoofdstuk 1 van dit proefschrift.

2. De veronderstelling, dat de in vaste waterstofhalogeniden optredende faseovergang van het λ-type samenhangt met het ontstaan van orde-over-lange-afstand, vindt steun in de resultaten van experimentele onderzoekingen naar het diëlectrische gedrag van deze stoffen.

J. Frenkel, *Kinetic Theory of Liquids* (Dover Publications, Inc., New York, 1955) p. 89.
Hoofdstuk 3 van dit proefschrift.

3. De met geconjugeerde richtingen werkende minimalisatiemethoden behoren tot de beste tot nu toe bekende numerieke technieken om extrema van functies met onbegrensde variabelen te bepalen.

R. Fletcher and C.M. Reeves, Computer Journal 7, 149 (1964).

4. Het moet mogelijk zijn uit de temperatuurafhankelijkheid van het Righi-Leduc-effect in uit lichte moleculen bestaande gassen, de karakteristieke rotatietemperatuur van deze gassen af te leiden.

5. Het gebruik van de Kramers-Kronig-betrekkingen in Fang's bewijsvoering voor het uniek zijn van dispersiefuncties van lineaire systemen werkt weinig verhelderend.

P.H. Fang, Physica 31, 1792 (1965).

6. Als benaming voor de kromme, welke gevormd wordt door het Cole-Cole-diagram, behorende bij de empirische Cole-Davidson dispersievergelijking, verdient de nauwkeurig gedefinieerde term "gegeneraliseerde lemniscaat" de voorkeur boven de vage term "scheve boog".

D.W. Davidson and R.H. Cole, J. Chem. Phys. 19, 1484 (1951).
H. Kober, *Dictionary of Conformal Representations* (Dover Publications, Inc., New York, 1957) p. 44.

7. De door Born geintroduceerde methode ter bepaling van de aggregatieneiging van thrombocyten is aan bedenkingen onderhevig.

G.V.R. Born and M.J. Cross, J. Physiol. 168, 178 (1963).

8. Het door Anderson en Reese voorgestelde mechanisme voor de fotochemische Fries-reactie is niet zinvol.

J.C. Anderson and C.B. Reese, J. Chem. Soc. London, 1781 (1963).

9. Wanneer een auteur in verschillende publicaties experimentele resultaten presenteert, welke niet met elkaar in overeenstemming zijn, mag hij een bespreking van deze discrepantie niet achterwege laten.

W. Dannhauser and R.H. Cole, J. Chem. Phys. 23, 1762 (1955).
W. Dannhauser and L.W. Bahe, J. Chem. Phys. 40, 3058 (1964).

10. Het zou aanbeveling verdienen te trachten de informatie, overeenkomstig Goudsmit's voorstel verkregen door registratie van wetenschappelijke uitspraken van slapende theoretici, aan belangstellenden eveneens tijdens hun slaap door te geven.

S.A. Goudsmit, Phys. Rev. Letters 15, 543 (1965).